Comparative ScRNA-Seq Profiling of Antigen-Specific CD4$^+$ T cells in Semi-Allogeneic Transplantation and Pregnancy Reveals Intersecting Signatures of Rejection and Tolerance

Michael S. Andrade[1], Grace Hynes[1], Zara Suran[1], Dengping Yin[1], Maria-Luisa Alegre[2], Peter T. Sage [3], Anita S. Chong[1*]

1. Section of Transplantation, Department of Surgery, The University of Chicago, 60637

2. Section of Rheumatology, Department of Medicine, The University of Chicago, 60637

3. Transplantation Research Center, Renal Division, Brigham and Women's Hospital, Harvard Medical School, 02115.

*Corresponding author: achong@bsd.uchicago.edu

SUMMARY

Transplantation tolerance without the need for lifelong immunosuppression is a central goal in transplant immunology yet prior sensitization events remain a major barrier to achieving stable tolerance. In reproductive immunology by contrast, pregnancy represents a spontaneous model of tolerance where the semi-allogeneic fetus evades rejection even in multiparous or previously sensitized mothers. $CD8^+$ T cell phenotypes of tolerance and rejection have been previously reported in transplant and pregnancy, but the transcriptional states of donor and fetus-specific $CD4^+$ T cells remain poorly defined. To address this, we performed Single-cell RNA-sequencing (ScRNA-seq) on endogenous, donor-specific $CD4^+$ T cells across models of naïve or paternally skin sensitized pregnancy as well as in a model of allogeneic heart transplants with or without co-stimulation blockade-induced tolerance. Our systems biology approach allowed us to identify shared and distinct transcriptional clusters of donor-specific $CD4^+$ *Foxp3*^{neg} T conventional (Tconvs) and *Foxp3*^{pos} regulatory (Tregs) T cells from peripheral lymphoid tissue. We expectedly found regulatory populations restricted to tolerance and pregnancy but were surprised to find significant overlap in activated follicular and non-follicular effector phenotypes in rejection and successful pregnancy. We also showed these murine populations were relevant and enriched in human datasets of health and disease respectively. These findings highlight context-dependent differentiation programs of antigen-specific $CD4^+$ T conventional and regulatory cells and provide new insights into their responses to allogeneic conflict at the intersection of transplant and reproductive immunology.

INTRODUCTION

Immune tolerance is a state of hyporesponsiveness towards self or non-self antigens [1]. Transplanted allogeneic organs invariably trigger immune-mediated rejection, which can broadly be classified as T cell mediated or antibody mediated, with emerging evidence that both frequently occur in settings of inadequate immunosuppression [2,3]. While pharmacological immunosuppression is the clinical standard of care to prevent rejection, the ability to induce lifelong transplantation tolerance through transient immunotherapy remains a central but elusive goal for the field. Multiple approaches, including co-stimulation blockade, can successfully induce transplantation tolerance in rodent models, however, translating them into clinical practice has represented a significant challenge [4]. High frequencies of alloreactive memory T and B cells represent a key barrier to the induction and maintenance of durable transplantation tolerance, but we lack a conceptual framework for reprograming these populations towards susceptibility to transplantation tolerance [5].

In contrast to transplantation, pregnancy is recognized as a spontaneous model of immunological tolerance whereby the maternal immune system accommodates the semi-allogeneic fetus despite expression of paternal antigens. This divergent immune responses to the semi-allogeneic fetus versus transplanted organs into immunologically competent adults was noted by Medawar in 1953 as an immunological paradox [6]. Multiple immune mechanisms contributing to tolerance of the semi-allogeneic fetus have been identified and can be classified into those acting locally at the maternal-fetal interface or systemically through the induction and

expansion of fetus-specific regulatory T cell (Treg), $CD8^+$ T cell exhaustion, and $CD4^+$ T cell tolerance through interactions with immunomodulatory B cells [7, 8, 9, 10, 11, 12].

In pregnancy, tolerance to the semi-allogenic fetus allows for successful parturition and repeated pregnancies, whereas in transplantation, exposure to the same alloantigen leads to immunological memory and accelerated rejection of a subsequent graft sharing the sensitizing antigen[13]. Indeed, we reported that prior sensitization to a single antigen expressed by the allograft was sufficient to destabilize transplantation tolerance [13]. The divergent immunological responses to allogeneic conflict prompted us to ask if reencounter of alloantigens in pregnancy following sensitization by paternal skin graft rejection would elicit a faster more rigorous recall immune response, or if pregnancy could dominantly constrain memory T cells. We reported that pregnancy was indeed able to override sensitization and program memory $CD8^+$ T cells toward states of exhaustion while also partially erasing features of memory. However, the transcriptional changes in antigen-specific naive and memory $CD4^+$ $Foxp3^{neg}$ T conventional cells (Tconvs) and $Foxp3^{pos}$ Tregs induced by transplantation and/or pregnancy have not been delineated.

Previous studies probing $CD8^+$ and $CD4^+$ T cell biology in pregnancy and transplantation have utilized bulk omics sequencing or TCR-transgenic T cells models, but these approaches are challenged by the innate heterogeneity driving T cell biology[14]. Single-cell RNA-sequencing (ScRNA-seq) approaches are beginning to elucidate novel populations of differentiating $CD4^+$ T cells [15,16] but investigation of polyclonal antigen-specific $CD4^+$ T cell populations at single cell resolution remains technically challenging due to their low frequencies. In this study, we applied ScRNA-seq to profile the transcriptomes of polyclonal, endogenous 2W:I-A^b tetramer-binding $CD4^+$ T cells that encountered the 2W peptide presented by mouse MHC class II I-A^b in settings of semi-allogeneic heart transplantation and pregnancy. Our studies reveal considerable heterogeneity in the $CD4^+$ T cell response, which was recapitulated across the models of acute rejection (Rej), anti-CD154-mediated transplant tolerance (Tol), naïve pregnancy at parturition (Pg), and pregnancy after rejection at parturition (sensitized pregnancy - SPg). We additionally show that these transcriptional rejection and tolerance responses are conserved in human $CD4^+$ T cells.

RESULTS

Donor-reactive $CD4^+$ T cells in transplantation rejection and Tolerance reveal divergent effector and regulatory signatures

C57BL/6 (B/6) mice received F1 (BALB/c x B/6) cardiac allografts expressing the model antigen, 2W-OVA (2W.F1)[17]. Naïve tolerant (Tol) allograft recipients were generated by the administration of donor splenocyte transfusion and anti-CD154 on the day of transplantation, followed by 2 additional anti-CD154 doses on post-operative days (POD) 7 and 14. Acute rejection (Rej) recipients received no treatment. Both groups of mice were sacrificed on POD30 and 2W-reactive $CD4^+$ T cells were identified with p2W:I-A^b tetramers and isolated by flow cytometry for ScRNA sequencing (**Fig. 1A**). We recovered approximately tenfold more $2W^+$ $CD4^+$ T cells from pooled Rej mice (n=2) compared to pooled Tol mice (n=6) (**Fig. S1A**).

We first performed pseudobulk analysis of the two transplant groups to reveal major differences between tolerance and rejection. This analysis revealed that *Satb1, Sell, Foxp3, Il2ra,*

and *Klrg1* were significantly upregulated in Tol consistent with a quiescent $CD4^+$ phenotype and Tregs as previously reported [13,18] (**Fig. 1B**). As expected, Rej upregulated *Cd44* as well as *Tnfsf8 (*CD30*), Lag3,* and *Itgb1(*Integrin beta 1*)* signaling antigen experience and activation. To assess heterogeneity across $CD4^+$ T cell populations, we applied UMAP dimensionality reduction. Unbiased clustering to generate nine distinct clusters across both conditions (**Fig. 1C)**. Using the top upregulated and downregulated differentially expressed genes (DEGs) (**Fig. 1D & Fig. S1B**) as well as a select group of markers, we annotated the clusters broadly based on lack of antigen experience (N), effector (E), follicular (F), regulatory (R), or unclassified (U) (**Fig. 1E**). Cluster N1 expressed the highest amount of *Sell* and *Satb1* while Cluster E1 represented a more quiescent effector memory population, marked by upregulation of *Crip1* but minimally expressing canonical effector cytokines like *Ifng or Tnf*. Cluster E2 showed a more activated phenotype, with top differentially expressed genes (DEGs) including *Tnfrsf8*, *Cd40lg*, *Ctla4*, and *Icos*, and Cluster E3 exhibited the most effector-like profile, with the highest *Ifng* and *Cd40lg* expression. Within the follicular category, clusters F1 and F2 co-expressed *Ifng* and *Il21* but *Il21* was higher, whereas Cluster F3 exhibited the highest expression of *Bcl6* and *Cxcr5*. The regulatory cluster R1 had the highest *Foxp3* expression as well as high *Ctla4* expression. Lastly, cluster U1 was proportionally similar in both groups and were enriched for splicing-associated genes such as *Srrm2*, *Utrn*, and *Lars2*, suggesting it may represent a transitional cluster.

Next, we investigated whether the function of these clusters could be further differentiated based on T cell receptor components (*Cd3*, *Cd4*, *Trac* and *Trbc2)* and *Thy1*. Overall, cluster E2 expressed the highest amount of *Trac*, cluster E3 exhibited higher expression of *Cd4* and *Thy1*, while F2 and F3 exhibited higher *CD3g* and *CD3e* respectively, compared to all other clusters. Importantly, these genes were comparably expressed at lower levels in clusters N1, R1, and U1 suggesting an increased expression of TCR signaling components associated with effector function in Tconvs (**Fig. S1C**).

To further interrogate the functional identity of each cluster, we performed Gene Ontology (GO) enrichment analysis. Cluster E1 was uniquely enriched for terms related to protein and molecular tag activity, E2 for TNF receptor binding, F2 for microtubule and tubule binding, U1 for histone-related activity, R1 for cytokine receptor activity, and F1 for double-stranded RNA binding (**Fig. S1D**). We additionally performed pathway enrichment using the Reactome database revealing our follicular clusters were most represented in TCR signaling pathways as well as antigen presentation pathways suggesting an ongoing antibody response, while the R1 cluster showed enrichment for interleukin signaling (**Fig. 1F**). Finally, to distinguish the two effector cluster categories more systematically, we applied pseudotime trajectory analysis (**Fig. S1E**). Despite their proximity in UMAP space, E2/E3 and F2/F3 resolved along distinct pseudotime trajectory branches. Notably, follicular clusters occupied the most advanced positions along pseudotime. (**Fig. S1F**).

Finally, demultiplexing of the biological groups from each cluster showed that Tol was dominated by antigen inexperienced cluster N1 and regulatory cluster R1 whereas Rej is dominated by the effector (E1-E3) and follicular (F1-3) clusters (**Fig. 1G**). Notably, Clusters E3 and F3 were restricted to Rej supporting the notion of rejection through donor-specific T cell and antibody responses. To further interrogate intra-cluster variability of gene expression we assessed multiple markers broadly classified as antigen experience, co-stimulatory/co-inhibitory and regulatory (**Fig. 1H**). Notably, Clusters E1, F1, and F2 present in Tol unexpectedly revealed expression of *Foxp3*, suggesting a unique propensity towards regulatory cells while sharing

effector and follicular transcriptomes of the E1, F1 and F2 clusters from Rej. Conversely, while Cluster R1 was overall phenotypically similar between both Tol and Rej groups, *Foxp, Il2ra, Il10*, and *Areg* expression was significantly higher in Tol compared to the same clusters from Rej. A further assessment of genes encoding transcription factors, activation, co-stimulatory, and co-inhibitory markers further advance our conclusion that Rej clusters were more activated (**Fig. S1G**), with all Rej clusters consistently exhibiting higher expression of activation markers such as *Tnfrsf4*, *Cd9*, and *Cd200* compared to the same Tol clusters, while the Rej follicular F1 and F2 clusters overexpressed *Gata3* and *Cd28*.

Pregnancy expands transcriptionally quiescent fetus-specific Tconvs and Tregs

To investigate the transcriptional consequences of pregnancy on donor-specific $CD4^+$ T cells, we crossed B/6 naïve virgin (NV) females with 2W-OVA BALB/c males. Spleens and lymph nodes were harvested on post-partum day 0–6 (Pg) or from NV controls, and 2W:I-A^b $CD4^+$ T cells were subject to ScRNA-seq (**Fig. 2A**). Pseudobulk analysis revealed upregulation of *Cd44*, *Ctla4*, and *Il7r* in the Pg group, consistent with antigen experience (**Fig. 2B**). UMAP projection and unbiased clustering revealed considerable transcriptional overlap between groups, and 4 naive-like (N1-4), 2 effector (E1 and E2), 1 Treg (R1) and 1 Unclassified (U1) cluster (**Fig. 2C**). Despite comparable cell recovery and quality control metrics between n=8 NV and n=4 Pg mice cluster frequency analysis showed an overall increase in the frequency of E2, R1 and U1 clusters in Pg compared to NV (**Fig. S2A**).

Cluster annotations based on top upregulated and downregulated DEGs revealed that all four N1-N4 clusters expressed *Sell* and *Satb1* indicating antigen inexperience. N1 was enriched for *Sox4* [19], N2 for the naïve T cell marker *Igfbp4* [20], and N3 for the negative regulator *Spred2* [21]—each consistent with a naïve-like phenotype (**Fig. 2D**, **Fig. S2B**). N4 had Interferon-induced protein with tetratricopeptide repeats 1 as a top upregulated gene, but *Sell* expression was high and *Cd44* expression low, so was characterized as naïve, as previously reported [22] (**Fig. 2E***)*. E1, was an effector γδ (gamma chain expression data not shown) T cell cluster expressing high *Ifng* and *Cd40lg*. The $\alpha\beta^+$ E2 cluster had the highest expression of *Cd44 and Itgb1* (VLA4ß) but minimally expressed *Tnf* and *Ifng*. R1 expressed highest amount of cannonical Treg genes including *Foxp3* and *Ctla4*. Cluster U1 lacked *Cd44* expression but expressed the splicing gene *Srrm2* [23], suggesting a splicing cluster with no differentiated phenotype. Assessment of the expression of T cell receptor components (*Cd3, Cd4, Trac* and *Trbc2)* and *Thy1* showed the Effector cluster E1 having the highest expression of *Thy1* and *Cd3e* and E2 the highest *Cd4* expression (**Fig. S2C**).

Gene Ontology enrichment revealed that E1 and E2 were enriched for cytokine and immune receptor activity as well as cytokine binding while R1 was mainly enriched for cytokine binding and cell adhesion processes (**Fig. S2D**). Focusing on the effector clusters, Reactome gene set enrichment analysis confirmed the effector nature of E1 with pathways for antigen presentation being among the most enriched while interleukin, alpha/beta signaling and co-stimulation pathways were most enriched in E2 (**Fig. 2F**). R1 was enriched for NF-κB and TNF-binding pathways suggesting a regulatory cluster receiving signals and poised for regulatory function. In line with findings from the functional gene set analysis, E1 and E2 were furthest along pseudotime, iterating their activated phenotype markers (**Fig. 2E**).

Finally, assessment of whether there was significant intra-cluster heterogeneity by biological group revealed that N1 was proportionally higher in NV, while E2 and R1 were

slightly higher proportionally in Pg (**Fig. 2G**). There were no major transcriptional differences in the N1-N4 clusters from Pg versus NV (**Fig. 2H**). Additionally, E2 clusters from Pg and NV were overall very similar to those from Pg having modestly lower expression of *Itga4, Cd9, and Nr4a1*. The R1 cluster was expanded in Pg but was overall transcriptionally similar to R1 from NV, with modestly elevated expression of *Cd44*, *Nt5e*, and *Ikzf2*. Thus, ScRNA-seq analysis showed that while pregnancy (in Pg) expanded the E2 and R1 clusters, they were remarkably similar transcriptionally to the same clusters from NV.

Pregnancy after sensitization imparts transcriptional traits of rejection and tolerance in antigen-specific Tconvs and Tregs

Given that acute rejection led to increased effector $CD4^+$ heterogeneity while pregnancy resulted in increased frequencies of quiescent effector and Treg populations, we examined the transcriptional response of antigen-specific $CD4^+$ T cells induced by pregnancy after rejection of skin grafts. To this end, B/6 virgin females were first sensitized by transplantation with 2W-OVA BALB/c skin. At 30–60 days after skin rejection, the mice were mated with 2W-OVA BALB/c males and these sensitized post-partum (SPg; n=4) mice were sacrificed on post-partum days 0–6 along with skin sensitized virgin controls (S; n=3) (**Fig. 3A**). Pseudobulk analysis revealed widespread upregulation of activation markers, TNF family genes, and cytokines in the SPg group while *Il7r* and *Satb1* were most prominent in the S group, consistent with enrichment of resting memory $CD4^+$ T cells (**Fig. 3B**).

Dimensionality reduction and clustering revealed heterogeneity in the $CD4^+$ cells, with distinct UMAP regions dominated by S or SPg (**Fig. 3C**). Unbiased clustering identified 11 clusters including an antigen-inexperienced N1 cluster (positive for *Sell, Satb1, Lef1, Igfbp, Cd44*^{neg}) and quiescent memory EM cluster (*Sell*^{low}, *Cd44*^{pos}, *Il7r*$^+$, *Ly6c2*$^+$) (**Fig. 3D-E & Fig. S3B**). E1 expressed *Mki67* highly suggesting a proliferating cluster, while the more dominant E2 expressed the most *CD44*, transcription factor, *Klf4*, but also *Foxp3*, and minimal *Tnf* and *Ifng*, suggestive of an atypical Th17-like cluster distinct from rejection [24]. Four follicular-like F1-F4 clusters were identified expressing varying levels of *Il21*, suggesting pregnancy permitting differentiation of $CD4^+$ T cells with specialized effector functions. The dominant F1 cluster expressed *Cd200* as one of its top DEGs, and co-expressed low levels *Tnf*, *Ifng* and *Il21*. F3 expressed the highest levels of the canonical Tfh genes, *Bcl6, Cxcr5, and Pdcd1* while F4 expressed the highest amount of *Il21, Ifng, and Ctla4.* Two *Foxp3*$^+$ Treg clusters were identified: a T follicular regulatory (FR) cluster that expressed *Foxp3, Bcl6, and Cxcr5* and a canonical Treg (R1) cluster that highly co-expressed *Foxp3* and *Ctla4.* Finally, an unclassified (U1) cluster was identified that lacked most canonical gene expression but was enriched for the splicing-associated gene *Son* [25].

Next, we assessed the expression of T cell receptor components and *Thy1* across clusters. T cell receptor genes (*Cd3e,Cd3g, Cd4, Trac,* and *Trbc2), with the E2, F1, F3 and F4 expressing the highest levels, similar to transplant responses* (**Fig. S3C**). Gene Ontology (GO) analysis revealed additional functional distinctions with E1 being overrepresented for microtubule-binding genes linked to proliferation and E2 being enriched for cytokine receptor and chemokine binding (**Fig. S3D**). GO biological processes overrepresentation analysis indicated that R1 overlapped with Tfh-like and non-Tfh effector, while FR showed greater similarity to R1 but lacked enrichment for canonical chemokine pathways, suggestive of distinct migratory patterns.

To validate the follicular identity of the F1-4 clusters, we scored all clusters using a curated "Full Tfh" gene module from *Podesta et al*, 2023 [14] and confirmed that all had positive module scores, with clusters F1 and F3 receiving the highest scores (**Fig. S3E).** Pseudotime trajectory analysis revealed that F1, F3, and E3 occupied distinct trajectory branches, consistent with divergent differentiation paths between Tfh and non-Tfh effectors, also observed in transplant rejection (**Fig. S3F**). To further interrogate overlap between follicular clusters F1 and F3 and non-follicular effectors E1 and E2, we enriched our clusters against the Reactome database (**Fig. 3F**). Cluster E2 was enriched more for IL-6 pathways while F1 was more enriched for immunoregulatory pathways and TNF binding. Congruent with the reported PD-1^+ expression by Tfh cells, PD-1 signaling was up in the follicular clusters F1 and F3 but not in E1 or E2 [26]. Taken together, our data suggest that some Tfh and non-Tfh clusters can be enriched for similar effector pathways but express different cell class markers, underscoring the complexity of $CD4^+$ differentiation pathways.

Finally, we interrogated intra-cluster heterogeneity between the S and SPg groups. S was dominated by the antigen-inexperienced cluster N1 and quiescent memory cluster EM, while six clusters (E2, F1, F3, F4, R1 and U1) were expanded in SPg (**Fig. 3G**). Antigen-inexperienced cluster N1 had high expression of *Sell* and *Satb1* while EM had higher expression of *Ikzf2* and *Itga4*, with both clusters from S and SPg being transcriptionally similar (**Fig. 3H & Fig. S3G**). Focusing on the clusters that expanded in SPg, E1 SPg had higher *Izkf2, Ctla4, Izumo1r, Tnfrsf4, and Casp3* while E2 SPg had higher *Cd40lg* expression compared to E1 and E2 from S, respectively. Notably, both SPg E1 and E2 did not have increased *Tnf* or *Ifn* compared to S, consistent with the lack of effector T cell differentiation that was observed in Rej.

The follicular cluster F1 SPg had higher *Il21, Ifng,* and *Cd40lg* than S which expressed higher *Sell* expression. F2 SPg had higher *Tnfrsf4* expression, as well as *Il21, Nt5e, Izumo1r,* and *Icos*. F3 and F4 were restricted to the SPg group also had high expression of these effector molecules. While both F3 and F4 clusters had high *Ikzf2* and *Tgfb1,* F3 had higher *Tox2* while F4 had higher *Il10, Il21, Ifng, Itga4, Casp3,* and *Lag3*. Collectively, these are indicative of ongoing pregnancy-specific Tfh responses.

Two $Foxp3^+$ Treg clusters were identified in our sensitized pregnancy model. The FR follicular regulatory cluster from S had higher *Sell, Foxp3, Il2ra, Bcl2* and *Nr4a1* as compared to SPg, hinting at a more activated state in SPg. R1 from S and SPg had mostly similar expression patterns except for S having higher *Gata3, Il2ra,* and *Il7r.* Finally, we noted that U1 SPg had increased expression of *Ikzf2, Izumo1r,* and *Nt5e*, which may point to a transitioning cell subset also observed in transplantation and naive pregnancy. Taken together, sensitized pregnancy was associated with increased heterogeneity in expanded Tconvs as well as activated Tregs that was reminiscent of rejection and tolerance respectively.

Conserved effector clusters from transplant and pregnancy mouse models are enriched in humans

We next tested whether the main effector clusters induced after transplant rejection (Tx-E2,-E3, -F2) were distinct from pregnancy effectors in Pg and SPg (**Fig. 4A**). Consistent with T cells experiencing rejection prior to pregnancy, SPg clusters were most transcriptionally enriched for all three effector Tx clusters, with the two dominant clusters, SPg-E2 and SPg-F1, having the highest module score for the Tx-E2 gene set (**Fig. 4B)**. The main Pg expanded non-Treg cluster,

Pg-E2, also had a higher module score for Tx-E2 transcriptome compared to Pg-N1, but the score was lower than SPg-E2. Individually examining the enrichment of SPg-E2 to Tx-E2 revealed a robust positive enrichment score of 0.751 (**Fig. 4C)**, whereas Pg-E2 had a negative enrichment score of -0.346, thus confirming similarity of SPg-E2 (but not Pg-E2) to Tx-E2 (**Fig. S4A).** Finally, Tx-E3 was the least enriched in both Pg and SPg (**Fig. S4B**). These observations support the conclusion that pregnancy does not induce the full differentiation of $CD4^+$ T cells to the mature effectors observed in transplant rejection.

Next, we focused on the Tx-F2 (Tfh-like cluster) and observed a positive enrichment of several SPg effector clusters while the sole Pg-E2 cluster was not enriched for Tx-F2, congruent with pregnancy-induced fetus-specific antibody (FSA) responses being a weaker and GC-independent response compared to the donor-specific antibody-responses (DSA) in Rej (**Fig. 4D)**[8]. SPg-F2 had the most positive enrichment of 0.773 consistent with a robust positive conserved follicular signature (**Fig. 4E)**. When the SPg non-Tfh clusters were compared to follicular Tx-F2, we unexpectedly noted that SPg-E1 was positively enriched (**Fig. S4C**) whereas S-E2 was negatively enriched (**Fig. S4D**). These data confirm that pregnancy in sensitized dams permits broad Tfh differentiation and resultant phenotypic overlap between differentiated $CD4^+$ Tconvs.

Finally, we confirmed that the transcriptional observations reflect protein expression by generating a spectral flow cytometry panel that probed for several T effector and follicular markers. To highlight the most dominant markers and phenotypes at the single cell resolution, we turned to Radviz visualization whereby markers are arranged along a circumference based on similarity of relative expression, and differentiated cells are positioned towards the most dominant markers and away from the center [27]. Overall, we found that Rej 2W:I-A^b Tconvs from the lymph nodes and spleen were similar to SPg Tconvs by marker polarization, with non-Tfh markers more polarizing in the spleen (**Fig. 4F**). Additionally, polarization of splenic Tconvs from both Rej and SPg towards the PE and APC tetramers suggest influence by avidity, which were diametrically opposed from the follicular markers, Bcl6 and Il21. Indeed, traditional flow gating confirms more tetramer MFI high cells are found in the spleen than lymph nodes informing the location of effector T cells with GC follicular T cells enriching in the lymph nodes and effector cells accumulating in the spleen (**Fig. S4E**).

We next tested whether the effector clusters of antigen-specific Tconvs in mice shared transcriptional profiles reported for human transplantation. Using a ScRNA dataset from kidney graft-infiltrating T cells at rejection (KTx) from *Shi et al, 2023* [28] we confirm that our mouse transplant (Tx) clusters E2, E3, and F2 were enriched for human kidney transplant rejection Tfh, Memory, and Th17 gene sets (**Fig. 4G**). Tx-E2 and Tx-F2 clusters had the highest module scores for KTx Tfh (**Fig. 4H**) and GSEA of Tx-E2 and Tx-F2 showed positive gene set enrichment scores (ES=0.35 and 0.335 respectively) for KTx Tfh (**Fig. 4I-J).** When compared to KTx Th17, Tx-E2 and Tx-E3 had modestly higher modules scores than the other mouse clusters (**Fig. 4K**), with positive enrichment of Tx-E2 cluster for KTx Th17 (ES=0.215), while Tx-E3 had a negative enrichment score (ES= -0.186), consistent with a lack of a robust Th17 signature in mouse heart transplant rejection (**Fig. S4F-G**). For the KTx Memory cluster, although Tx-E3 had the highest module score it was not statistically significant but Tx-F3 was significantly lower than Tx-F2 suggesting Tx-F3 is not a memory follicular response consistent with an on-going antibody response (**Fig. S4H**). Finally, since we examined a human gene set of transplant rejection, we asked if our pregnancy clusters were enriched for a human dataset from *Moldenhauer et al, 2024*

[29] of Tconvs from Early Pregnancy Failure. Consistent with successful pregnancies in both our mouse models, they were not (**Fig. S4I**).

Heterogeneous follicular T cells associated with alloantibody responses in acute rejection and pregnancy after transplant rejection

The conserved follicular signature across our models and in human was associated with strong anti-fetus (2W and B/c) IgG responses in SPg that were higher than anti-donor (2W and B/c) IgG responses in Rej and S (**Fig. 5A**). To test for conserved Tfh phenotypes in the Rej and SPg groups, we performed a sub-analysis of $CD4^+$ Tfh-like cells expressing *Bcl6*, *Cxcr5*, *Il21*, or *Pdcd1* from Rej and SPg samples (**Fig. 5B**). Nine follicular-like clusters were identified and verified to be "bona fide" follicular T cells based on module scores against a published "Full Tfh" gene set from *Podesta et al, 2023* [14]. All clusters, except SF and P1, demonstrated high enrichment (**Fig. 5C**). Differential gene expression analysis revealed that SF was enriched for the splicing and apoptosis-associated [31] gene *Lars2* suggesting a transitioning state (**Fig. 5D & Fig. S5A**). Enrichment analysis using "Progenitor, Tfh versus Tfr, and Tfr" gene sets from *Podesta et al, 2023* [14] and *Huo et al, 2019* [32] confirmed P1 as a progenitor-like cluster and pFR as Tfr, with the remaining clusters were consistent with conventional Tfh phenotypes (**Fig. S5B**).

Cluster proportion analysis revealed a single rejection (rF4) cluster dominant in Rej while SPg had three increased clusters, pF5, pF6, and pFR (**Fig. 5E**). We focused on these clusters, as the other clusters were progenitor cells or comparably low frequency in Rej and SPg (**Fig. 5F**). We analyzed a select list of effector markers and noted that the transplant-dominant rF4 expressed high *Il7r* and *Itga4* consistent with a more memory-like state, which could be explained by these T cells being analyzed on D30 post-transplantation after allograft rejection on ~D10-12 [13]. In contrast, pF5, pF6, and pFR were identified from SPg on D0-6 post-parturition when the anti-fetus IgG response was still increasing [8]. pF5 expressed more *Lag3* and *Tgfb1* compared to pF6 and rF4, but less than pFR (**Fig. 5G**). Overexpression of *Lag3* and *Tgfb1* is reminiscent of $Foxp3^-$ $Il10^+$ TR1 cells prompting us to test whether the pF5 cluster was enriched for TR1-related genes. Indeed, pF5 was higher than rF4 and pF6 for many TR1-associated genes including *Il10* (**Fig. 5H**). Using a TR1-specific gene set from *Solé et al, 2023* [33], we confirm that Cluster pF5 and pFR were positively enriched for TR1 genes, with scores of ES=0.477 and 0.458 respectively (**Fig. 5I, Fig. S5D**) whereas pF6 and rF4 were negatively enriched (**Fig. 5J**, **Fig. S5E)**. Notably, both pF5 and pFR exhibited the highest number of predicted cell-cell interactions, supporting their regulatory identity (**Fig. S5F**). A direct comparison of the most differentially expressed genes revealed that despite a shared TR1 signature, pF5 more highly expressed *CD30*, *Ifng*, *Il21*, and *Cd200* compared to pFR, while pFR was enriched for regulatory genes *Foxp3* and *Ikzf2*, thus reinforcing potentially distinct regulatory cell populations in SPg (**Fig S5G**).

A phylogenetic tree based on average gene expression revealed that follicular $CD4^+$ T cell heterogeneity could be placed on a divergent spectrum, ultimately leading to Tfh-like or Tfr/TR1-like phenotypes (**Fig. 5K**). Pseudotime and RNA velocity analyses corroborated this divergence, with pregnancy-dominant pF6 and pFR further along pseudotime than transplant-dominant rF4 (**Fig. S5H**). These pF6, pFR and rF4 clusters also diverged in intronic velocity directionality reflecting the complexity of the $CD4^+$ response in SPg as a result of heterogeneity in the Tfh and regulatory responses (**Fig. 5L, Fig. S5I**).

Resolving Foxp3$^+$ Treg heterogeneity in transplantation and pregnancy

Expanded clusters of *Foxp3*$^+$ T cells in Tol, Pg, and SPg prompted a focused analysis on whether they were transcriptionally conserved across pregnancy and co-stimulation blockade-induced transplantation tolerance (**Fig. 6A**). Clustering revealed distinct enrichment of 6 clusters that were annotated based on canonical markers, and heterogenous expression of *Foxp3* (**Fig. 6B-C & Fig. S6A**). Each experimental group harbored at least 4 clusters, with quiescent Central Tregs dominant in Tol and S (at 30-60 days post-sensitization with skin graft). Unexpectedly, despite ten-fold fewer *Foxp3*$^+$ cells recovered from Rej, the proportion of Treg clusters in Tol and Rej were similarly dominated by *Foxp3*-high and Effector-high clusters and an additional expanded Tfr cluster in Rej. In contrast, Pg was dominated by central Tregs, with the remaining 40% comprising *Foxp3*-high, Effector-high and Tfr clusters. Most remarkable was pregnancy in sensitized dams (SPg), which resulted in the expansion of all 5 non-central Treg clusters where the dominant clusters were Effector-low, Effector-high and Tfr.

Differential gene expression analysis confirmed that Central Tregs were most antigen inexperienced and expressed *Sell* but not *CD44*, while proliferating Tregs showed strong cell cycle signatures including *Mki67*. The *Foxp3* High cluster was uniquely *Mif* negative and enriched for splicing genes. Follicular Tregs expressed *Bcl6* and *Cxcr5*, Effector-low Tregs upregulated S100-family genes while Effector-high Tregs highly expressed genes implicated in Treg function including *Entpd1, Gzmb, Itgae, Il10, Klrg1*, and higher *Tcf7* and *Tnfrsf11*(**Fig. 6D-E & Fig. S6B***)*. GO enrichment confirmed these annotations (**Fig. 6F**), and TCR/CD3/CD4 genes were most abundant in the Follicular and Effector High/Low clusters (**Fig. S6C**). A deeper look at functional, adhesion, co-stimulatory/co-inhibitory, and follicular genes revealed that the Effector-High Tregs expressed more functional Treg genes than Effector-Low, Follicular, and proliferating Tregs, despite sharing expression of many other markers (**Fig. 6G**). Trajectory analysis suggested that Proliferating Tregs bifurcate into Follicular or Effector-Low lineages, with the latter transitioning into Effector-High cells (**Fig. S6D**). Intronic RNA velocity analysis highlighted *Foxp3* High Tregs as having the highest pseudotime (**Fig. S6E**) suggesting increased transcriptional priming, while gene-specific RNA velocity plots (e.g., *Itga4* and *Klrg1*) impute an effector-like trajectory (**Fig. S6F**).

To evaluate transcriptional similarity across transplantation (Tx) and pregnancy in naive (Pg) versus sensitized (SPg) mice, we compared their Treg gene sets. Module score and GSEA enrichment against the transplant-derived Tx-R1 cluster revealed that while both Pg-R1 and SPg-R1 showed positive enrichment, SPg-R1 was more enriched (**Fig. 6H–I & Fig. S6G**). Within the SPg clusters, predicted cell-cell interactions revealed that R1 and E1 had the highest interaction counts, although E1 was a minor subset (**Fig. S6H, Fig. 3G**). Notably, the R1 and F5 (Tr1-enriched) clusters exhibited strong incoming and outgoing interaction strength, suggesting Tregs were highly interactive during pregnancy of sensitized dams (**Fig. S6I**).

Conserved transplantation and pregnancy Foxp3$^+$ clusters are preferentially enriched in lymphoid organs and human datasets

Tregs function to dampen T cell priming in secondary lymphoid organs in LNs and spleen [34]. Thus, we compared our dataset with a reference ScRNA-seq study from *Miragaia et al, 2019* [35] that defined the transcriptomes of lymphoid tissue-specific Treg states in mice. Our

antigen-specific Central, Effector-Low, Effector-High, and Follicular Tregs were enriched in the Miragaia splenic Treg gene signatures, while the Proliferating and to a lesser extent, Follicular Tregs, aligned with Miragaia brachial lymph node effector signatures (**Fig. 7A**). Notably, our Central Tregs had a high positive enrichment score of 0.867 (**Fig. 7B**) and a robust positive module score (**Fig. S7A**), indicative of a conserved resting Treg signature in secondary lymphoid organs. When scored against the Miragaia splenic effector gene set, our Effector-High and -Low Treg clusters showed strong positive module scores while the Proliferating and *Foxp3* High clusters were only modestly enriched (**Fig. 7C**). Finally, our Proliferating cluster had a positive module score and positive enrichment for the Brachial lymph node effector gene set (**Figs. S7B & S7C**).

We next conducted cross-species validation using a healthy human peripheral blood Treg dataset from *Luo et al, 2021* [36], which also revealed conserved signatures. Our Proliferating cluster had the highest module score (**Fig S7D**) and was positively enriched for the human MKI67^{hi} population (ES=0.65; **Fig. 7E**), while our *Foxp3* High cluster was positively enriched for the human *FOXP3*^{hi} subset (ES=0.412; **Fig. 7F**). Our Effector-Low cluster corresponded closely to the Activated/Effector subset is congruent with the human Treg gene set being derived from healthy donors and our Effector-Low cluster being prevalent in naive mice (**Fig. 7G–H**). We also compared our Treg clusters to gene sets from peripheral blood Tregs derived from human acute Graft vs Host Disease (GVHD) patients, which were classified as activated or proliferating. We now observed high enrichment and module enrichment scores for our Proliferating, Effector and Follicular Tregs for the GVHD Activated Tregs, and our Proliferating Tregs were most enriched for the GVHD Proliferating Tregs (**Fig S7E-F**). These observations further confirming conserved activation and proliferating Tregs signatures across species as well as health and disease states.

To further validate Treg responses in pregnancy, we enriched our clusters against a gene set of unstable Tregs associated with Early Pregnancy Failure [29]. However, we observed no module score enrichment in any of our Tregs clusters suggesting our Treg clusters were stable (**Fig. S7G**). As such, next probed the transcriptome of healthy, pregnancy-specific Tregs and found *Wienke et al,* [37] reported a gene set of activated, maternal uterine Tregs which we used for enrichment. Effector High cluster had the highest module scores followed by the Effector Low, (**Fig. 7I**) which was recapitulated by GSEA enrichment score of 0.26 and 0.182, respectively (**Figs. S7H and S7I**). These data suggest that stable Tregs in successful pregnancy are transcriptionally conserved in mice and humans and can be distinguished from unstable human Tregs.

Based on the findings of Wienke et al. [37] that *Ox40* was a conserved activation marker of uterine Tregs during pregnancy, we examined Ox40 as well as a select group of effector and follicular markers on Tregs from Pg and SPg. From both lymph node and spleen, Radviz visualization of these flow cytometry markers confirmed Ox40 and Foxp3 were grouped next to each other indicating co-expression. It also revealed that Pg Tregs were polarized toward an OX40^{+} phenotype, whereas SPg Tregs displayed dual Ox40^{+} and Bcl6^{+} polarization (**Fig. 7J)**, consistent with SPg Tregs having the greatest representation of Effector-High and Follicular subsets. These observations support the conclusion that sensitized pregnancy elicits the most functionally diverse and activated Tregs that are similarly reflected in the spleen and lymph node.

DISCUSSION

Herein, through ScRNA phenotyping and a systems biology approach, we demonstrate distinct and overlapping heterogeneity of endogenous, antigen-specific $CD4^+$ T cell responses to heart transplant, pregnancy, and pregnancy after transplant rejection. Transplant rejection was characterized by follicular and non-follicular effectors, whereas transplant tolerance was associated with the expansion of a canonical *Foxp3*$^+$ Treg cluster. These follicular and non-follicular effectors were enriched in a human kidney-infiltrating gene set of rejecting patients highlighting the relevance and overlapping phenotype between mice and humans in rejection. A surprising observation was that in Tol but not Rej, the same follicular and non-follicular effector clusters expressed *Foxp3*, while conversely, the Treg cluster from Rej had lower *Foxp3* expression than from Tol. These observations underscore a potential shortcoming of unbiased clustering distinguishing Tconvs from Tregs but more importantly highlight the potential implication of a singular master transcription factor difference despite strong phenotypic overlap between rejection and tolerance phenotypes. Whether these cells share activated phenotypes but divergent effector or regulatory functions or are transitioning to becoming iTregs or ex-Tregs requires further studies [38].

In our naïve pregnancy model, we observed modest expansion of effector and regulatory *CD44*$^+$ cells with 4 of 8 clusters expressing antigen-inexperienced markers: *Sell* and *Satb1*. These results highlight the divergent $CD4^+$ responses to allogeneic conflict in pregnancy and transplantation, where both by frequency and activation phenotype, pregnancy effectively constrains effector populations. In fact, compared to effector clusters in our transplant model, the *Cd44*$^+$ effectors in naïve pregnancy were remarkably similar to the same cluster from naive virgin. More specifically, naïve pregnancy effector cluster E2 lacked an *Ifng*$^+$ signature or regulatory markers such as *Il10* and *Areg* observed in the E1, E2, E3 clusters from our transplant rejection and tolerance models, respectively. Our articulation of these atypical effector $CD4^+$ T cells will hopefully pave the way for their better characterization in other contexts of immune hypofunction.

In contrast to naive pregnancy, successful parturition in sensitized pregnancy requires the control of antigen-specific memory $CD4^+$ responses generated during the rejection of allogeneic skin. Skin-sensitized mice were dominated by an *Il7r*$^+$ memory cluster, while a compendium of effector Tconvs and Tregs was observed in SPg. Effector-like non-Tfh and Tfh clusters were induced in sensitized pregnancy, and protein expression with Radviz visualization confirmed $IL21^+$ and $IL21^-$ polarization of Tconvs in both spleen and lymph nodes. The two Tfh-like clusters restricted to sensitized pregnancy is congruent with a strong anti-fetus IgG response. Importantly, SPg E2 and Tfh clusters were transcriptionally enriched for Tx effector and Tfh clusters, as well as for ScRNA gene sets of human graft-infiltrating Tfh-like cells from kidney transplant rejection [28]. That peripheral follicular signatures enrich within a human *in-situ* gene set illustrates the relevance of effector heterogeneity articulated in mouse models.

Additional sub-analysis of pooled follicular T cells from Rej and SPg revealed two regulatory, Tfr and TR1-like, clusters. Others have reported that TR1 cells can emanate from Tfh cells [33, 39], thus underscoring the ability of pregnancy in sensitized dams to simultaneously elicit both regulatory follicular and TR1-like clusters not observed in Rej, Tol or Preg. We speculate that the Tfr populations may emerge to constrain Tfh responses in SPg and may

emanate from either Tregs or Tfh to control T effector cells or promote B cell differentiation into Bregs [40, 41, 42, 43, 44].

The constraint of mature, effector $CD4^+$ T cells is likely attainable through both cell-intrinsic and cell-extrinsic mechanisms exerted by $Foxp3^+$ Tregs or other regulatory cells [45]. Cell-intrinsic loss of function can be due to T cell anergy and exhaustion, with anergy arising from TCR priming without co-stimulation and exhaustion induced by persistent antigen exposure [46]. Transcriptional analysis of these two hypofunctional states have identified heterogenous phenotypes without coalescing to a conserved signature. Reduced AP-1 (activator protein 1), Fos/Jun-containing NF-AT complexes, and inactive NF-kB complexes comprising p50 homodimers, have been implicated in anergy [47]. *Trefzer et al* reported that persistently activated CD4 T cells upregulate the exhaustion markers Lag3, PD1, CD209, and the anergic feature of FR4/CD73 coexpression and modulated MAPK, mTORC,1 and calcineurin signaling pathways [46]. Finally, recent studies on oral tolerance reported expanded endogenous polyclonal antigen-specific $CD4^+$ T cells that fell into five subsets that were naive-like, $CXCR5^+$ T follicular helper-like, or $FR4^{pos}CD73^{pos}$ Th-lineage-negative ($Thlin^-$) anergic cells [48]. Our studies identified two (E1 and E2) clusters in SPg, and an E2 cluster in Preg that do not upregulate lineage-defining effector genes, *Tnf, Ifng, Bcl6, Cxcr5* or *Il21*, but instead, upregulate *Izumo1r, Nt5e, Ctla4, Nrp1, Ikzf2* and *Tnfrsf18* also expressed by anergic, follicular *and* $Foxp3^+CD4^+$ T cells . However, while the SPg E1-3 clusters share multiple markers with the SPg Tfh clusters, by trajectory and RNA velocity analyses, the E1, E2, F1 and F3 sub-populations appeared along different branches and had divergent velocity directionality suggesting they are not converging into a common phenotype. Therefore, whether the atypical effectors identified in Pg and SPg represents the elusive exhausted or anergic $CD4^+$ T cells from previous studies remains to be investigated. Notably, these clusters were not present in anti-CD154-induced transplantation tolerance, suggesting a distinct mechanism for constraining $CD4^+$ cells that leans towards regulation by $Foxp3^+$ Tregs.

Observations of a critical role of $Foxp3^+$ Tregs playing critical roles in transplantation and pregnancy tolerance prompted [7, 8, 9, 10, 11, 12, 13] a deeper analysis of $Foxp3^+$ cells concatenated across all models, and which revealed substantial Treg heterogeneity. Central Tregs, most represented in our control groups and substantially reduced in SPg, overlapped with published quiescent mouse and human Tregs. The SPg group exhibited strong representation across all other Treg clusters, suggesting a diversified regulatory landscape unique to this group. Effector-Low Tregs expressed several S100 family proteins as top upregulated DEGs; S100 proteins are responsible for signaling cascades of immune functions including motility, inflammation, and differentiation [49]. Effector-Low Tregs lacked the effector molecules expressed by Effector-High Tregs, however, increasing *Il10* expression in the Proliferating and Effector-Low Tregs suggests the possibility of the former clusters maturing into Effector-High Tregs. Consistent with this, trajectory analysis revealed a shared branch spanning Proliferating, Effector-Low and Effector-High Tregs. Interestingly, while the $Bcl6^+Cxcr5^+$ Follicular, Effector-Low and Effector-High Tregs co-expressed genes mediating regulation, *Tgfb1, Nt5e* and *Areg*, follicular Tregs did not upregulate effector genes unique to Effector-High Tregs. These observations underscore distinct effector phenotypes for the distinct Treg clusters [50].

Finally, we describe a Foxp3 High cluster with robust *Foxp3, Ikzf2, and Tgfb1* expression that co-expressed several splicing genes as top upregulated DEGs. Indeed, throughout our transplant and pregnancy models we consistently identified an “Unclassified” cluster expressing

the genes *Srrm2* and *Lars2* that are involved in RNA splicing of immature into mature RNA, and protein synthesis through tRNA charging and mTORC1 activation, respectively [23, 25, 51]. We speculate that the Foxp3 High is a transitioning cluster. Consistent with this hypothesis, *Itga4*, a migration associated molecule [52], and *Klrg1*, which were highly expressed in the Effector High Treg cluster, had positive RNA velocity in the Foxp3 High cluster suggesting increased nascent mRNA for these markers. Deciphering the trajectory and phenotype of effector Tregs will be useful in better articulating Treg phenotypes in disease pathology versus health.

Importantly, we show conserved signatures of our mouse Tregs with published human Tregs, namely our proliferating Tregs corresponded with a proliferating Treg gene set in healthy human donors and GVHD patients. Furthermore, our Effector-Low and -High Tregs corresponded with human effector Tregs from uterine tissues in healthy pregnancy. By protein and Radviz visualization, we confirmed that the conserved marker Ox40 was present in all our Tregs in both spleen and lymph nodes and a key polarizing marker of activated Tregs. Finally, our Treg clusters were not enriched for a Treg gene set derived from Early Pregnancy Failure patients with a disrupted Treg transcriptional signatures. These observations illustrate the utility of our phenotypic approach for identifying Tregs signatures with sufficient granularity to classify Tregs across health and disease.

In its totality, our ScRNA analysis across murine models of transplantation and pregnancy reveals the extent of heterogeneity in antigen-specific $CD4^+$ Tconvs and Tregs. Specifically, across our models we unveiled two types of effector Tregs, a discrete Tfr population, and a TR1-like population restricted to sensitized pregnancy which we speculate are contributing to successful tolerance and parturition. Our analysis reinforced two types of $CD4^+$ effectors across our models: Tfh and Non-Tfh. We highlighted a collection of effector markers which overlapped or were distinct in each type. Regardless of whether these are temporary effector states along an effector continuum or more permanent states, we foresee these cluster phenotypes being useful in annotating future $CD4^+$ T cell subsets. Our ScRNA dataset should also contribute to functional and surveillance studies where the tolerance and rejection phenotypes we uncovered can serve as a template of biomarkers to monitor for pregnancy loss, transplant rejection risk, or to potentially desensitize patients [53] for better transplant outcomes. We anticipate our dataset will be helpful not only to T cell biologists in transplantation and reproductive immunology but also to other settings where tolerance mechanisms need to be better defined.

Limitations of the Study

Pregnancy is a complex, carefully orchestrated biological process involving various biological systems with distinctly described phases [54], but we restricted our study to one portion of this process, namely at parturition. Similarly, transplantation in both tolerance and rejection is marked by distinct phases (early vs late) that can affect T cell phenotype, but we restricted our study to POD30. In addition, we did not interrogate graft-infiltrating and fetal/maternal interface lymphocytes. However, we reasoned that pooling cells from spleen and lymph nodes would allow us to make broad comparisons as it reports T cell biology in the periphery across models. Despite pooling multiple mice for each experimental condition in each model, the recovery of low cell numbers could lead to sampling error in some groups. While low recovery is a reality of profiling an endogenous, antigen-specific population, the ScRNA-seq approach nevertheless

allowed us to assess the transcriptome at a per cell basis across transplantation and pregnancy. Finally, while we highlighted multiple populations, we did not perform functional analyses to verify whether our profiled clusters were functionally regulatory, dysfunctional, or rejecting in a transplant or pregnancy context. Instead, we leveraged canonical markers from the literature to annotate clusters and the models themselves, where the known fate of the transplanted organ or success of the pregnancy, allowed us to generate hypotheses of their function. Future studies will focus on validating the function, complexity, and balance of the clusters we defined.

ACKNOWLEDGEMENTS

We thank the University of Chicago Flow Core and Single Cell Immunophenotyping Core as well as the Animal Resource Center for their animal husbandry services. We also thank the NIH Tetramer Core Facility for providing all the tetramers used in this study (contract number 75N93020D00005). This work was supported by grants from the NIH (P01AI097113, R01AI182097, R01AI148705) to ASC, MLA and PTS.

AUTHOR CONTRIBUTIONS

MSA conceptualized, constructed, and scripted all ScRNA-seq libraries and bioinformatics analysis pipelines. MSA designed all tissue-processing and antibody-staining protocols. MSA, GH, and ZS prepared mice, processed tissue, and performed flow cytometry experiments. DY performed heart and skin transplants. MLA and PTS provided critical feedback on data analysis. MSA and ASC designed the study, generated the figures, and cowrote the manuscript. All authors edited the manuscript.

MATERIALS AND METHODS

Mice

C57BL/6 (B6) and BALB/c (B/c) females, ages 7-8 weeks, were purchased from the Jackson Laboratory or Harlan Laboratories. 2W-OVA B/c males were crossed with B6 females to generate 2W-OVA F1 mice which were used as heart transplant donors. 2W-OVA B/c females were used as skin transplant donors. 2W-OVA B/c males were crossed with virgin B6 females to generate naïve post-partum mice. To generate sensitized post-partum mice, Virgin B6 females transplanted with 2W-OVA skin were bred with 2W-OVA B/c males at post-operative D30-60. Mouse experiments were approved by the Institutional Animal Care and Use Committee at the University of Chicago using standards of the NIH *Guide for the Care and Use of Laboratory Animals* (National Academies Press, 2011).

Tissue Processing

Spleens and inguinal, axial, and brachial lymph nodes were harvested and passed through a 40 μM strainer (Corning, catalog 431750). Lymphocytes were enriched for $CD4^+$ (Miltenyi Biotec, catalog 130-104-454) cells by negative selection prior to antibody staining. Samples were stained

for flow cytometry using LiveDead NearIR (Invitrogen, Thermo Fisher Scientific) to exclude dead cells. An antibody cocktail was used to exclude unwanted cells, consisting of CD49b (DX5, catalog 485971-82, Invitrogen, Thermo Fisher Scientific), CD11c (N418, catalog 48-0114-82), F4/80 (BM8, catalog 48-4801-82, Invitrogen, Thermo Fisher Scientific), NK1.1 (PK136, catalog 48-5941-82 eBioscience, Thermo Fisher Scientific), Ter-119 (Ter-119, catalog 48-5921-82, eBioscience, Thermo Fisher Scientific), and CD19 (eBio1D3, catalog 48-0193-82, Invitrogen, Thermo Fisher Scientific). Additional antibodies for phenotyping against CD90.2 (53-2.1, 565257, BD Biosciences), CD4 (GK1.5, 612952, BD Biosciences), Foxp3 (FJK-16s, catalog 53-5773-82, Invitrogen, Thermo Fisher Scientific), Bcl-6 (358509, Biolegend), Icos (117427, Biolegend), CD200/Ox2 (123817, Biolegend), Itga4 (103611, Biolegend), CD27 (124233, Biolegend), IL21 (48-7211-82, Thermo), Cxcr5 (752549, BD), CD134/OX40 (119411, Biolegend), Cxcr4/CD184 (146517, Biolegend), Ccr7/CD197 (120127, Biolegend), CD279/PD-1 (135241, Biolegend), and PD-L1 (569606, BD) were used to stain T cells. The NIH Tetramer Facility provided PE and APC-conjugated 2W (EAWGALANWAVDSA):I-A^b tetramers. Tetramer stains were incubated for 40 minutes at room temperature prior to the addition of all other antibodies. The FACSAria Fusion (BD) was used for cell sorting or the Cytek Aurora (Cytek Biosciences) was used to quantify flow cytometry experiments. Cells were fixed and permeabilized if intracellular stains were required.

Donor/Fetal-specific antibody quantification

Donor/Fetal-specific antibodies in the serum of post-partum mice or post-transplanted mice were measured using 1×10^6 BALB/c or 2W-OVA B6 splenocytes which were incubated for 30 minutes at 4°C with 2 μL of serum from recipient mice. Cells were then washed and incubated with anti-CD19 (1D3, catalog 550992, BD Biosciences) and goat anti-mouse IgG (H+L) (catalog 1031-02, Southern Biotech) for 30 minutes at 4°C. MFI of the $CD19^-$ cells that were IgG positive was measured by flow cytometry on the Cytek Aurora.

ScRNA Library Construction and Processing

Single cell suspensions of lymphoid tissue from each biological group were stained with distinct barcoded antibodies (Cell-Hashtag Oligonucleotides, TotalSeq-B, Biolegend) and sorted on CD90.2+CD4+ double 2W+ tetramer positive (PE and APC) cell surface markers at the University of Chicago Flow Cytometry Core. The 10x Chromium was used in the University of Chicago Single Cell Immunophenotyping Core. Single cell 3' Kit v3.1 Dual Index Gene Expression with Feature Barcoding, 10x Genomics kit was used to generate cDNA, mRNA, and hashtag oligonucleotide (HTO) libraries per manufacturer's directions. The 3' mRNA libraries were sequenced up to 40,000 reads per cell while the HTO libraries to at least 5000 reads per cell using a Novaseq 6000 SP Flow cell. Fastq files from bcl files were generated using Cell Ranger mkfastq and alignment was performed using the STAR aligner against the mm10 transcriptome. Cell Ranger outputs were loaded into Seurat for further QC exclusion of cells > 25% mitochondrial reads.

Bioinformatics

Standard Seurat processing workflow was used with top n=6000 most variable genes used for PCA generation. Unbiased clusters were generated using the FindClusters command with a resolution of 0.7 for all datasets. Uniform Manifold Approximation and Projection (UMAP) was used for dimensionality reduction taking the top n=20 dimensions from the PCA analysis for all datasets. Differentially expressed genes (DEGs) were found using the FindAllMarkers command using default parameters. Module scores were computed using the AddModuleScore function using default parameters. Pseudotime trajectory analysis was performed using the Monocle3 package while Cell-Cell interaction analysis was performed with CellChat using the filterCommunication function with a minimum of n=5 cells. ClusterProfiler was used for Gene Ontology (GO) overrepresentation analysis. AUCell from the SeuratExtend package was used to calculate gene set enrichment analysis scores (GSEA) against custom gene sets as well as the Reactome database with default parameters. Radviz Analysis was performed using the Radviz package according to the default workflow. Briefly, MFI data from each cell of flow cytometry fcs files was exported to R and normalized, markers were used to generate anchors, and the cosine similarity was used to optimize the position of the anchors.

Statistics

Statistical calculations were made using R or GraphPad Prism Version 10.2.3. *P*-values below 0.05 were considered significant. For pairwise comparisons and the FindAllMarkers function we used the Wilcoxon rank sum test and for multiple pairwise comparisons we used the Holm method to adjust p-values. For DSA calculation we used an ordinary two-way ANOVA using Tukey's multiple comparisons test.

FIGURE LEGENDS

Figure 1: 2W-OVA*:*I-A^{b} CD4^{+} T Cells from Naïve Tolerant heart transplant recipients are enriched for *Foxp3*$^{+}$ while Acute Rejecting 2W-OVA:I-Ab CD4^{+} T Cells are enriched for effector follicular and non-follicular populations

A. Experimental design of 2W-OVA-F1 heterotopic allograft transplanted into NaiveTol (with MR1/DST at D0, 7, and D14) recipient or Acute Rejecting (no immunosuppression) and sacrificed at post-operative D30.
B. Pseudobulk volcano plot of differentially expressed genes (DEGs) by 2W-OVA*:*I-A^{b} CD4^{+} T Cells from Rej and Tol.
C. Dimensionality reduction UMAP split by biological groups, Rej and Tol (top), or nine unbiased clusters (bottom).
D. Top n=3 upregulated DEGs in each cluster.
E. Dot-plot of select canonical markers for CD4^{+} T cell subsets expressed by each cluster.
F. Heatmap of effector clusters by z-score of top enriched Reactome Database "Immune System" pathways of Mus musculus.
G. Bar plot of proportion of unbiased clusters in each experimental group.

H. Violin plot by cluster split by biological group of canonical marker genes categorized as antigen experience, co-stimulatory/co-inhibitory, effector, follicular, and regulatory.

Supplemental Figure 1: Extended transcription analysis of 2W-OVA*:*I-A^{b} CD4^{+} T Cells from transplant Tol vs Rej

A. Total Recovery, number of cells that passed QC, and percentage breakdown of each unbiased cluster by biological group in Rej or Tol 2W-OVA*:*I-A^{b} CD4^{+} T Cells. Cells pass QC if <25% mitochondrial reads and nFeature_RNA>100.
B. Top n=3 downregulated DEGs in each cluster.
C. Scaled heatmap of T cell receptor components and T cell lineage gene, Thy1.
D. Overrepresentation analysis of Gene Ontology terms by cluster.
E. Trajectory and pseudotime analysis overlaid on UMAP.
F. Barplot of Pseudotime ordering by cluster.
G. Violin plot by clusters based on experimental groups, and their expression of select transcription factors and activation/co-stimulatory/co-inhibitory molecules.

Figure 2: 2W-OVA*:*I-A^{b} CD4^{+} T Cells in Naïve Pregnancy are enriched for an effector and a *Foxp3*$^{+}$ cluster

A. 2W-OVA BALB/c male breeders were crossed with Naïve (N) virgin C57BL/6 females to generate Naïve post-partum (Pg) mice that were sacrificed on post-partum D0-6.
B. Pseudobulk volcano plot of differentially expressed gene by 2W-OVA*:*I-A^{b} CD4^{+} T Cells from NV and Pg.
C. Dimensionality reduction UMAP with indicated biological group (top) and eight unbiased clusters (bottom).
D. Top n=3 upregulated DEGs in each cluster.
E. Dot plot of select canonical markers in each clusters.
F. Heatmap of effector clusters by z-score of top enriched Reactome Database “Immune System” pathways of Mus musculus.
G. Bar plot of proportion of unbiased clusters in each experimental group.
H. Violin plot by cluster split by biological group of canonical marker genes categorized as antigen experience, co-stimulatory/co-inhibitory, effector, follicular, and regulatory.

Supplemental Figure 2: Extended transcription analysis of 2W-OVA*:*I-A^{b} CD4^{+} T Cells from NV vs Pg

A. Total Recovery, number of cells that passed QC, and percentage breakdown of each unbiased cluster by biological group in Rej or Tol 2W-OVA*:*I-A^{b} CD4^{+} T Cells. Cells pass QC if <25% mitochondrial reads and nFeature_RNA>100.
B. Top n=3 downregulated DEGs in each cluster.
C. Scaled heatmap of T cell receptor components and T cell lineage genes.
D. Over-representation analysis of Gene Ontology terms by cluster.
E. Trajectory and pseudotime analysis overlaid on UMAP.

F. Violin plot by clusters based on experimental groups, and their expression of select transcription factors and activation/co-stimulatory/co-inhibitory molecules.

Figure 3: Skin Sensitized Skin Sensitized Post-Partum mice expand 2W-OVA*:*I-A^{b} CD4^{+} T Cells into heterogenous effector and regulatory phenotypes

A. 2W-OVA BALB/c male breeders were crossed with 2W-OVA skin sensitized mice (S) at post-operative D30-60 to generate Sensitized post-partum (SPg) mice sacrificed between 0-6 days after parturition.
B. Pseudobulk volcano plot of DEGs by 2W-OVA*:*I-A^{b} CD4^{+} T Cells from S and SPg.
C. Dimensionality reduction UMAP with indicated biological group (top) and 11 unbiased clusters (bottom).
D. Top n=3 upregulated DEGs in each cluster.
E. Dot plot of select canonical markers by clusters.
F. Heatmap of effector clusters by z-score of top enriched Reactome Database "Immune System" pathways of Mus musculus.
G. Bar-plot of proportion of unbiased clusters in each experimental group.
H. Violin plot by cluster split by biological group of canonical marker genes categorized as antigen experience, co-stimulatory/co-inhibitory, effector, follicular, and regulatory.

Supplemental Figure 3: Extended transcription analysis of 2W-OVA*:*I-A^{b} CD4^{+} T Cells from S vs SPg

A. Total Recovery, number of cells that passed QC, and cluster breakdown by biological group in S or SPg 2W-OVA*:*I-A^{b} CD4^{+} T Cells. Cells pass QC if <25% mitochondrial reads and nFeature_RNA>100.
B. Top n=3 downregulated DEGs in each cluster.
C. Scaled heatmap of T cell receptor components and T cell lineage genes.
D. Overrepresentation analysis of Gene Ontology terms by cluster.
E. Module score of *Sage et al. 2023* "Full Tfh" gene list overlaid on UMAP.
F. Trajectory and pseudotime analysis overlaid on UMAP.
G. Violin plot by clusters based on experimental groups, and their expression of select transcription factors and activation/co-stimulatory/co-inhibitory molecules.

Figure 4: Gene set enrichment analysis of *Foxp3*- 2W-OVA*:*I-A^{b} CD4^{+} Tconvs in transplant and pregnancy clusters for mouse and human datasets

A. Heatmap of scaled enrichment of Naïve pregnancy (from NV & Pg) and Sensitized pregnancy (from S & SPg) effector clusters against transplant (from Rej + Tol) effector clusters.
B. Module score of Naïve pregnancy (from NV & Pg) and Sensitized pregnancy (from S & SPg) effector clusters against transplant effector cluster Tx-E2 (from Rej & Tol).
C. Gene Set Enrichment Analysis (GSEA) of S-E2 (from S & SPg) enriched for Tx-E2.

D. Module score of Naïve pregnancy (from NV & Pg) and Sensitized pregnancy (from S + SPg) effector clusters against transplant effector cluster Tx-F2 (from Rej & Tol).
E. GSEA of S-F2 (from S&SPg) enriched for Tx-F2.
F. Radviz of Rej and SPg *Foxp3*- 2W-OVA*:*I-A^b CD4$^+$ from the lymph nodes or spleen, showing flow cytometry protein expression for follicular, effector, and 2W-OVA tetramer markers (PE and APC).
G. Heatmap of scaled enrichment of transplant clusters (from Rej & Tol) against *Shi et al.* [28] graft-infiltrating clusters of kidney transplant rejection patients.
H. Module score enrichment of transplant clusters (from Rej & Tol) enriched for *Shi et al.* [28] "Tfh" CD4$^+$ gene set.
I. GSEA of Tx-E2 (from Rej & Tol) enriched for *Shi et al.* [28] "Tfh" CD4$^+$ gene set.
J. GSEA of Tx-F2 (from Rej & Tol) enriched for *Shi et al.* [28] "Tfh" CD4$^+$ gene set.
K. Module score enrichment of transplant clusters (from Rej & Tol) enriched for *Shi et al.* [28] "Th17" CD4$^+$ gene set.

Supplemental Figure 4: Extended gene set enrichment analysis of *Foxp3*- 2W-OVA*:*I-A^b CD4$^+$ transplant and pregnancy clusters for mouse and human datasets

A. GSEA of N-E2 (from NV & Pg) enriched for our Tx-E2 (from Rej & Tol) gene set.
B. Module score of Naïve pregnancy (from NV & Pg) and Sensitized pregnancy (S & SPg) effector clusters against transplant effector cluster E3 (from Rej & Tol).
C. GSEA of S-E1 (from S & SPg) enriched for our Tx-F2 (from Rej & Tol) gene set.
D. GSEA of S-E2 (from S & SPg) enriched for our Tx-F2 (from Rej & Tol) gene set.
E. PE and APC MFI of 2W-OVA*:*I-A^b tetramer binding to Tconvs from the spleen or lymph nodes of Rej and SPg.
F. GSEA of Tx-E2 (from Rej & Tol) enriched for the *Shi et al.* [28] "Th17" CD4$^+$ gene set.
G. GSEA of Tx-E3 (from Rej & Tol) enriched for the *Shi et al.* [28] "Th17" CD4$^+$ gene set.
H. Module score of transplant clusters (from Rej & Tol) enriched for *Shi et al.* [28] "Memory" CD4$^+$ gene set.
I. Module score of Naïve pregnancy (from NV & Pg) and Sensitized pregnancy (from S & SPg) effector clusters against *Moldenhauer et al.* [29] "Early Pregnancy Failure TConvs" (EPF) gene set.

Figure 5: Acute Rejection and Sensitized Pregnancy elicit distinct 2W-OVA*:*I-A^b CD4$^+$ Follicular T cell phenotypes

A. Mean Fluorescence Intensity (MFI) of anti-2W-OVA and anti-B/c IgG in the sera from Naïve, Rej, S, and SPg.
B. UMAP of 2W-OVA*:*I-A^b CD4$^+$ Follicular T Cells by unbiased clusters. Cells were subset as: Bcl6>0 or Cxrc5>0 or Il21 >0 or Pdcd1 >0.
C. Violin plot of module score by clusters against *Podesta et al.*[15] "Tfh Full" gene set.
D. Top n=3 upregulated DEGs by cluster.
E. Bar plot of unbiased clustering broken down by biological group.
F. Violin plot of select Follicular marker genes including canonical, progenitor, and regulatory expressed by each unbiased cluster.
G. Scaled heatmap of select effector markers for clusters rF4, pF5, pF6, and pFR.

H. Scaled heatmap of select TR1-related markers for clusters rF4, pF5, pF6.
I. GSEA of pF5 on *Solé et al.*[33] TR1-Specific gene set.
J. GSEA of pF6 on *Solé et al.* [33] TR1-Specific gene set.
K. Phylogenetic tree of average gene expression by cluster.
L. Proportion of cells from biological group in each cluster.

Supplemental Figure 5: Extended transcription analysis, Cell-Cell interaction, Trajectory, and RNA Velocity analysis of Follicular 2W-OVA*:*I-A^b CD4$^+$ T Cells in Acute Rejection (Rej) and Sensitized Pregnancy (SPg)

A. Top n=3 downregulated differentially expressed genes (DEGs) by cluster.
B. UMAP and Module score against "Progenitor" (*Podesta et al.*[15]), "Tfh vs Tfr" (*Hou et al.* [32]), and "Tfr" (*Hou et al.* [32]) gene sets.
C. Scaled heatmap of gene set enrichment for *Solé et al.* [33].
D. GSEA of pFR on *Solé et al.* [33] TR1-Specific gene set.
E. GSEA of rF4 on *Solé et al.* [33] TR1-Specific gene set.
F. Number of CellChat Cell-Cell interactions by cluster.
G. Waterfall plot of DEGs from pF5 and pFR.
H. Trajectory and pseudotime analysis overlaid on UMAP.
I. RNA Velocity by cluster overlaid on UMAP.

Figure 6: *Foxp3*$^+$ 2W-OVA*:*I-A^b CD4$^+$ Subset Analysis across transplantation and pregnancy

A. 2W-OVA*:*I-A^b CD4$^+$ T Cells with reads of *Foxp3*>0 from all biological groups were re-clustered and annotated.
B. Stacked barplot of *Foxp3*$^+$ Clusters by biological group.
C. Ridgeplot of *Foxp3* expression for each annotated cluster.
D. Heatmap of top n=10 upregulated differentially expressed genes.
E. Violin plot by cluster of select Regulatory marker genes including antigen experience, canonical regulatory, transcription factors (TFs), STAT Proteins, and activation/function.
F. Overrepresentation analysis dotplot of Gene Ontology terms by cluster.
G. Violin plot by cluster of select Regulatory marker genes including antigen experience, canonical regulatory, transcription factors (TFs), STAT Proteins, and activation/function.
H. Module score of select clusters from naïve pregnancy (N-N1 and N-R1) and sensitized pregnancy (S-N1 and S-R1) against our transplant *Foxp3*$^+$ cluster (Tx-R1).
I. GSEA of S-R1 on Tx-R1

Supplemental Figure 6: Extended transcription analysis, Cell-Cell interaction, Trajectory, and RNA Velocity analysis of *Foxp3*$^+$ 2W-OVA*:*I-A^b CD4$^+$ clusters

A. Violin plot of select markers used for cluster annotations.
B. Heatmap of top n=10 downregulated DEGs.
C. Dotplot of T cell receptor and T cell lineage gene expression by cluster.
D. Trajectory and pseudotime analysis overlaid on UMAP.

E. Intronic RNA Velocity pseudotime of clusters.
F. RNA velocity of *Itga4* and *Klrg1*.
G. GSEA of N-R1 on Tx-R1.
H. Number of CellChat Cell-Cell interactions by cluster of S + SPg groups only.
I. CellChat relative outgoing/incoming interaction strength by cluster of S + SPg groups only.

Figure 7: Gene set enrichment analysis of *Foxp3*$^+$ 2W-OVA:I-A^b CD4$^+$ clusters from transplant and pregnancy for mouse and human Treg datasets

A. Scaled heatmap by cluster of enrichment for the *Miragaia et al.* [35] gene set.
B. GSEA of Central Tregs on *Miragaia et al.* [35] "Splenic Central Tregs."
C. Module score of clusters against *Miragaia et al.* [35] "Splenic Effector Tregs."
D. Scaled heatmap by cluster of enrichment for the *Luo et al.* [36] "Healthy Donor Tregs" gene set.
E. GSEA of Proliferating Tregs on *Luo et al.* [36] "MKI67 Hi" gene set.
F. GSEA of *Foxp3* High Tregs on *Luo et al.* [36] "*FOXP3* Hi" gene set.
G. GSEA of Effector Low Tregs on *Luo et al.* [36] "*FOXP3* Activated/Effector" gene set.
H. GSEA of Effector High Tregs on *Luo et al.* [36] "*FOXP3* Activated/Effector" gene set.
I. Module score of clusters against *Wienke et al.* [37] "Maternal Uterine Tregs."
J. Radviz of Pg and SPg *Foxp3*$^+$ Tregs from lymph node or spleen.

Supplemental Figure 7: Extended gene set enrichment analysis of *Foxp3*$^+$ 2W-OVA:I-A^b CD4$^+$ clusters from transplant and pregnancy for mouse and human Treg datasets

A. Module score of clusters against *Miragaia et al.* [35] "Splenic Central Tregs."
B. Module score of clusters against *Miragaia et al.* [35] "Brachial Lymph Node Effector Tregs."
C. GSEA of Proliferating Tregs on *Miragaia et al.* [35] "Brachial Lymph Node Effector Tregs."
D. Module score of clusters against *Luo et al.* [36] "Healthy Donor Proliferating Tregs."
E. Scaled heatmap by cluster of enrichment for the *Luo et al.* [36] "Graft Vs Host Disease Tregs."
F. Module score of clusters against *Luo et al.* [36] "GVHD Activated Tregs."
G. Module score of clusters against *Moldenhauer et al.* [29] "Early Pregnancy Failure TRegs" gene set.
H. GSEA of Effector Low Tregs on *Wienke et al.* [37] "Maternal Uterine Tregs."
I. GSEA of Effector High Tregs on *Wienke et al.* [37] "Maternal Uterine Tregs."

REFERENCES

1. Han, L., Wu, T., Zhang, Q., Qi, A., and Zhou, X. (2025). Immune Tolerance Regulation Is Critical to Immune Homeostasis. Journal of Immunology Research *2025*, 5006201. https://doi.org/10.1155/jimr/5006201.

2. Ruiz, P., Maldonado, P., Hidalgo, Y., Gleisner, A., Sauma, D., Silva, C., Saez, J.J., Nuñez, S., Rosemblatt, M., and Bono, M.R. (2013). Transplant tolerance: new insights

and strategies for long-term allograft acceptance. Clin Dev Immunol *2013*, 210506. https://doi.org/10.1155/2013/210506.

3. Callemeyn, J., Lamarthée, B., Koenig, A., Koshy, P., Thaunat, O., and Naesens, M. (2022). Allorecognition and the spectrum of kidney transplant rejection. Kidney International *101*, 692–710. https://doi.org/10.1016/j.kint.2021.11.029.

4. Pinelli, D., and Ford, M. Novel Insights into Anti-CD40/CD154 Immunotherapy in Transplant Tolerance: Immunotherapy: Vol 7 , No 4 - Get Access. https://www.tandfonline.com/doi/full/10.2217/imt.15.1.

5. Karahan GE, Claas FHJ and Heidt S (2020) Pre-existing Alloreactive T and B Cells and Their Possible Relevance for Pre-transplant Risk Estimation in Kidney Transplant Recipients. *Front. Med.* 7:340. doi: 10.3389/fmed.2020.00340

6. Medawar P.B. (1953). Some immunological and endocrinological problems raised by the evolution of viviparity in vertebrates. Symp Soc Exp Biol. *7*, 320–338.

7. Kinder, J.M., Turner, L.H., Stelzer, I.A., Miller-Handley, H., Burg, A., Shao, T.-Y., Pham, G., and Way, S.S. (2020). CD8+ T Cell Functional Exhaustion Overrides Pregnancy-Induced Fetal Antigen Alloimmunization. Cell Reports *31*. https://doi.org/10.1016/j.celrep.2020.107784.

8. Suah, A.N., Tran, D.-K.V., Khiew, S.H.W., Andrade, M.S., Pollard, J.M., Jain, D., Young, J.S., Yin, D., Chalasani, G., Alegre, M.-L., et al. (2021). Pregnancy-induced humoral sensitization overrides T cell tolerance to fetus-matched allografts in mice. J Clin Invest *131*. https://doi.org/10.1172/JCI140715.

9. Lewis, E.L., Xu, R., Beltra, J.-C., Ngiow, S.F., Cohen, J., Telange, R., Crane, A., Sawinski, D., Wherry, E.J., and Porrett, P.M. (2021). NFAT-dependent and -independent exhaustion circuits program maternal CD8 T cell hypofunction in pregnancy. Journal of Experimental Medicine *219*, e20201599. https://doi.org/10.1084/jem.20201599.

10. Pollard, J.M., Hynes, G., Yin, D., Mandal, M., Gounari, F., Alegre, M.-L., and Chong, A.S. (2024). Pregnancy dedifferentiates memory $CD8^+$ T cells into hypofunctional cells with exhaustion-enriched programs. JCI Insight *9*. https://doi.org/10.1172/jci.insight.176381.

11. Rizzuto, G., Brooks, J.F., Tuomivaara, S.T., McIntyre, T.I., Ma, S., Rideaux, D., Zikherman, J., Fisher, S.J., and Erlebacher, A. (2022). Establishment of fetomaternal tolerance through glycan-mediated B cell suppression. Nature *603*, 497–502. https://doi.org/10.1038/s41586-022-04471-0.

12. Kalekar, L.A., Schmiel, S.E., Nandiwada, S.L., Lam, W.Y., Barsness, L.O., Zhang, N., Stritesky, G.L., Malhotra, D., Pauken, K.E., Linehan, J.L., et al. (2016). CD4+ T cell

anergy prevents autoimmunity and generates regulatory T cell precursors. Nat Immunol *17*, 304–314. https://doi.org/10.1038/ni.3331.

13. Andrade, M.S., Young, J.S., Pollard, J.M., Yin, D., Alegre, M.-L., and Chong, A.S. (2022). Linked sensitization by memory $CD4^+$ T cells prevents costimulation blockade–induced transplantation tolerance. JCI Insight *7*. https://doi.org/10.1172/jci.insight.159205.

14. Osum KC, Jenkins MK. Toward a general model of $CD4^+$ T cell subset specification and memory cell formation. Immunity. 2023 Mar 14;56(3):475-484. doi: 10.1016/j.immuni.2023.02.010. PMID: 36921574; PMCID: PMC10084496.

15. Podestà, M.A., Cavazzoni, C.B., Hanson, B.L., Bechu, E.D., Ralli, G., Clement, R.L., Zhang, H., Chandrakar, P., Lee, J.-M., Reyes-Robles, T., et al. (2023). Stepwise differentiation of follicular helper T cells reveals distinct developmental and functional states. Nat Commun *14*, 7712. https://doi.org/10.1038/s41467-023-43427-4.

16. Zhang, H., Podestà, M.A., Cavazzoni, C.B., Wu, Y., Lee, J.-M., Li, X., Raeder, P.L., Chandrakar, P., Gempler, M., Richardson, S., et al. (2025). Follicular regulatory T cells restrain kidney allograft rejection in mice by suppressing alloreactive B cells. Nat Commun *16*, 2151. https://doi.org/10.1038/s41467-025-57468-4.

17. Burns, A.M., Ma, L., Li, Y., Yin, D., Shen, J., Xu, J., and Chong, A.S. (2009). Memory Alloreactive B Cells and Alloantibodies Prevent Anti-CD154-Mediated Allograft Acceptance. The Journal of Immunology *182*, 1314–1324. https://doi.org/10.4049/jimmunol.182.3.1314.

18. Delacher, M., Imbusch, C.D., Hotz-Wagenblatt, A., Mallm, J.-P., Bauer, K., Simon, M., Riegel, D., Rendeiro, A.F., Bittner, S., Sanderink, L., et al. (2020). Precursors for Nonlymphoid-Tissue Treg Cells Reside in Secondary Lymphoid Organs and Are Programmed by the Transcription Factor BATF. Immunity *52*, 295-312.e11. https://doi.org/10.1016/j.immuni.2019.12.002.

19. Kuwahara, M., Yamashita, M., Shinoda, K., Tofukuji, S., Onodera, A., Shinnakasu, R., Motohashi, S., Hosokawa, H., Tumes, D., Iwamura, C., et al. (2012). The transcription factor Sox4 is a downstream target of signaling by the cytokine TGF-β and suppresses TH2 differentiation. Nat Immunol *13*, 778–786. https://doi.org/10.1038/ni.2362.

20. Elyahu, Y., Hekselman, I., Eizenberg-Magar, I., Berner, O., Strominger, I., Schiller, M., Mittal, K., Nemirovsky, A., Eremenko, E., Vital, A., et al. (2019). Aging promotes reorganization of the CD4 T cell landscape toward extreme regulatory and effector phenotypes. Science Advances *5*, eaaw8330. https://doi.org/10.1126/sciadv.aaw8330.

21. Sun, C., Fujisawa, M., Ohara, T., Liu, Q., Cao, C., Yang, X., Yoshimura, T., Kunkel, S.L., and Matsukawa, A. (2022). Spred2 controls the severity of Concanavalin A-induced

liver damage by limiting interferon-gamma production by CD4+ and CD8+ T cells. Journal of Advanced Research *35*, 71–86. https://doi.org/10.1016/j.jare.2021.03.014.

22. Zemmour, D., Kiner, E., and Benoist, C. (2020). CD4+ teff cell heterogeneity: the perspective from single-cell transcriptomics. Current Opinion in Immunology *63*, 61–67. https://doi.org/10.1016/j.coi.2020.02.004.

23. Xu, S., Lai, S.-K., Sim, D.Y., Ang, W.S.L., Li, H.Y., and Roca, X. (2022). SRRM2 organizes splicing condensates to regulate alternative splicing. Nucleic Acids Research *50*, 8599–8614. https://doi.org/10.1093/nar/gkac669.

24. An, J., Golech, S., Klaewsongkram, J., Zhang, Y., Subedi, K., Huston, G.E., Wood III, W.H., Wersto, R.P., Becker, K.G., Swain, S.L., et al. (2011). Krüppel-like factor 4 (KLF4) directly regulates proliferation in thymocyte development and IL-17 expression during Th17 differentiation. The FASEB Journal *25*, 3634–3645. https://doi.org/10.1096/fj.11-186924.

25. Lu, X., Ng, H.-H., and Bubulya, P.A. (2014). The role of SON in splicing, development, and disease. WIREs RNA *5*, 637–646. https://doi.org/10.1002/wrna.1235.

26. Shi, J., Hou, S., Fang, Q., Liu, X., Liu, X., and Qi, H. (2018). PD-1 Controls Follicular T Helper Cell Positioning and Function. Immunity *49*, 264-274.e4. https://doi.org/10.1016/j.immuni.2018.06.012.

27. Abraham, Y., Gerrits, B., Ludwig, M.-G., Rebhan, M., and Gubser Keller, C. (2017). Exploring Glucocorticoid Receptor Agonists Mechanism of Action Through Mass Cytometry and Radial Visualizations. Cytometry Part B: Clinical Cytometry *92*, 42–56. https://doi.org/10.1002/cyto.b.21499.

28. Shi, T., Burg, A.R., Caldwell, J.T., Roskin, K.M., Castro-Rojas, C.M., Chukwuma, P.C., Gray, G.I., Foote, S.G., Alonso, J.A., Cuda, C.M., et al. (2023). Single-cell transcriptomic analysis of renal allograft rejection reveals insights into intragraft TCR clonality. J Clin Invest *133*. https://doi.org/10.1172/JCI170191.

29. Moldenhauer, L.M., Foyle, K.L., Wilson, J.J., Wong, Y.Y., Sharkey, D.J., Green, E.S., Barry, S.C., Hull, M.L., and Robertson, S.A. (2024). A disrupted FOXP3 transcriptional signature underpins systemic regulatory T cell insufficiency in early pregnancy failure. iScience *27*, 108994. https://doi.org/10.1016/j.isci.2024.108994.

30. Liu, W., Zhao, J., Kang, Z.-Y., Xiao, Y.-L., Yang, L., Liu, C., and Li, D.-H. (2021). De novo donor-specific HLA antibodies reduce graft survival rates and increase the risk of kidney transplant rejection: A single-center retrospective study. Transplant Immunology *68*, 101430. https://doi.org/10.1016/j.trim.2021.101430.

31. Feng, S., Wan, S., Liu, S., Wang, W., Tang, M., Bai, L., and Zhu, Y. (2022). LARS2 Regulates Apoptosis via ROS-Mediated Mitochondrial Dysfunction and Endoplasmic

Reticulum Stress in Ovarian Granulosa Cells. Oxidative Medicine and Cellular Longevity *2022*, 5501346. https://doi.org/10.1155/2022/5501346.

32. Hou, S., Clement, R.L., Diallo, A., Blazar, B.R., Rudensky, A.Y., Sharpe, A.H., and Sage, P.T. (2019). FoxP3 and Ezh2 regulate Tfr cell suppressive function and transcriptional program. Journal of Experimental Medicine *216*, 605–620. https://doi.org/10.1084/jem.20181134.

33. Solé, P., Yamanouchi, J., Garnica, J., Uddin, M.M., Clarke, R., Moro, J., Garabatos, N., Thiessen, S., Ortega, M., Singha, S., et al. (2023). A T follicular helper cell origin for T regulatory type 1 cells. Cell Mol Immunol *20*, 489–511. https://doi.org/10.1038/s41423-023-00989-z.

34. Campbell, C., and Rudensky, A. (2020). Roles of Regulatory T Cells in Tissue Pathophysiology and Metabolism. Cell Metabolism *31*, 18–25. https://doi.org/10.1016/j.cmet.2019.09.010.

35. Miragaia, R.J., Gomes, T., Chomka, A., Jardine, L., Riedel, A., Hegazy, A.N., Whibley, N., Tucci, A., Chen, X., Lindeman, I., et al. (2019). Single-Cell Transcriptomics of Regulatory T Cells Reveals Trajectories of Tissue Adaptation. Immunity *50*, 493-504.e7. https://doi.org/10.1016/j.immuni.2019.01.001.

36. Luo, Y., Xu, C., Wang, B., Niu, Q., Su, X., Bai, Y., Zhu, S., Zhao, C., Sun, Y., Wang, J., et al. (2021). Single-cell transcriptomic analysis reveals disparate effector differentiation pathways in human Treg compartment. Nat Commun *12*, 3913. https://doi.org/10.1038/s41467-021-24213-6.

37. Wienke, J., Brouwers, L., Burg, L.M. van der, Mokry, M., Scholman, R.C., Nikkels, P.G.J., Rijn, B.B. van, and Wijk, F. van (2020). Human Tregs at the materno-fetal interface show site-specific adaptation reminiscent of tumor Tregs. JCI Insight *5*. https://doi.org/10.1172/jci.insight.137926.

38. Shevach, E.M., and Thornton, A.M. (2014). tTregs, pTregs, and iTregs: similarities and differences. Immunological Reviews *259*, 88–102. https://doi.org/10.1111/imr.12160.

39. Roncarolo, M.G., Gregori, S., Bacchetta, R., Battaglia, M., and Gagliani, N. (2018). The Biology of T Regulatory Type 1 Cells and Their Therapeutic Application in Immune-Mediated Diseases. Immunity *49*, 1004–1019. https://doi.org/10.1016/j.immuni.2018.12.001.

40. Sage PT, Sharpe AH. The multifaceted functions of follicular regulatory T cells. Curr Opin Immunol. 2020 Dec;67:68-74. doi: 10.1016/j.coi.2020.10.009. Epub 2020 Oct 24. PMID: 33176227; PMCID: PMC7744352.

41. Jacobsen JT, Hu W, R Castro TB, Solem S, Galante A, Lin Z, Allon SJ, Mesin L, Bilate AM, Schiepers A, Shalek AK, Rudensky AY, Victora GD. Expression of Foxp3 by T follicular helper cells in end-stage germinal centers. Science. 2021 Jul 16;373(6552):eabe5146. doi: 10.1126/science.abe5146. Epub 2021 Jul 15. PMID: 34437125; PMCID: PMC9007630.

42. Roncarolo MG, Gregori S, Bacchetta R, Battaglia M, Gagliani N. The Biology of T Regulatory Type 1 Cells and Their Therapeutic Application in Immune-Mediated Diseases. Immunity. 2018 Dec 18;49(6):1004-1019. doi: 10.1016/j.immuni.2018.12.001. PMID: 30566879.

43. Solé P and Santamaria P (2021) Re-Programming Autoreactive T Cells Into T-Regulatory Type 1 Cells for the Treatment of Autoimmunity. *Front. Immunol.* 12:684240. doi: 10.3389/fimmu.2021.684240

44. Clemente-Casares, X., Blanco, J., Ambalavanan, P. *et al.* Expanding antigen-specific regulatory networks to treat autoimmunity. *Nature* **530**, 434–440 (2016). https://doi.org/10.1038/nature16962

45. Reinhardt, J., Sharma, V., Stavridou, A., Lindner, A., Reinhardt, S., Petzold, A., Lesche, M., Rost, F., Bonifacio, E., and Eugster, A. (2022). Distinguishing activated T regulatory cell and T conventional cells by single-cell technologies. Immunology *166*, 121–137. https://doi.org/10.1111/imm.13460.

46. Trefzer, A., Kadam, P., Wang, S.-H., Pennavaria, S., Lober, B., Akçabozan, B., Kranich, J., Brocker, T., Nakano, N., Irmler, M., et al. (2021). Dynamic adoption of anergy by antigen-exhausted CD4+ T cells. Cell Reports *34*. https://doi.org/10.1016/j.celrep.2021.108748.

47. Sundstedt, A., Sigvardsson, M., Leanderson, T., Hedlund, G., Kalland, T., and Dohlsten, M. (1996). In vivo anergized CD4+ T cells express perturbed AP-1 and NF-kappa B transcription factors. Proceedings of the National Academy of Sciences *93*, 979–984. https://doi.org/10.1073/pnas.93.3.979.

48. Hong, S.-W., Krueger, P.D., Osum, K.C., Dileepan, T., Herman, A., Mueller, D.L., and Jenkins, M.K. (2022). Immune tolerance of food is mediated by layers of CD4+ T cell dysfunction. Nature *607*, 762–768. https://doi.org/10.1038/s41586-022-04916-6.

49. Singh, P., and Ali, S.A. (2022). Multifunctional Role of S100 Protein Family in the Immune System: An Update. Cells *11*, 2274. https://doi.org/10.3390/cells11152274.

50. Li, H., Fang, R., Ma, R., Long, Y., He, R., Lyu, H., Chen, L., and Wen, Y. (2024). Amphiregulin promotes activated regulatory T cell-suppressive function via the AREG/EGFR pathway in laryngeal squamous cell carcinoma. Head & Face Medicine *20*, 62. https://doi.org/10.1186/s13005-024-00466-6.

51. Cui, H., Diedrich, J.K., Wu, D.C. *et al.* Arg-tRNA synthetase links inflammatory metabolism to RNA splicing and nuclear trafficking via SRRM2. *Nat Cell Biol* **25**, 592–603 (2023). https://doi.org/10.1038/s41556-023-01118-8

52. Glatigny, S., Duhen, R., Arbelaez, C., Kumari, S., and Bettelli, E. (2015). Integrin alpha L controls the homing of regulatory T cells during CNS autoimmunity in the absence of integrin alpha 4. Sci Rep *5*, 7834. https://doi.org/10.1038/srep07834.

53. Leal R, Pardinhas C, Martinho A, Sá HO, Figueiredo A, Alves R. Strategies to Overcome HLA Sensitization and Improve Access to Retransplantation after Kidney Graft Loss. J Clin Med. 2022 Sep 28;11(19):5753. doi: 10.3390/jcm11195753. PMID: 36233621; PMCID: PMC9572793.

54. Pandey, M.K. (2024). Immunological harmony: the dynamic influence of cellular and humoral immunity on pregnancy success. Discov. Immun. *1*, 2. https://doi.org/10.1007/s44368-024-00002-3.

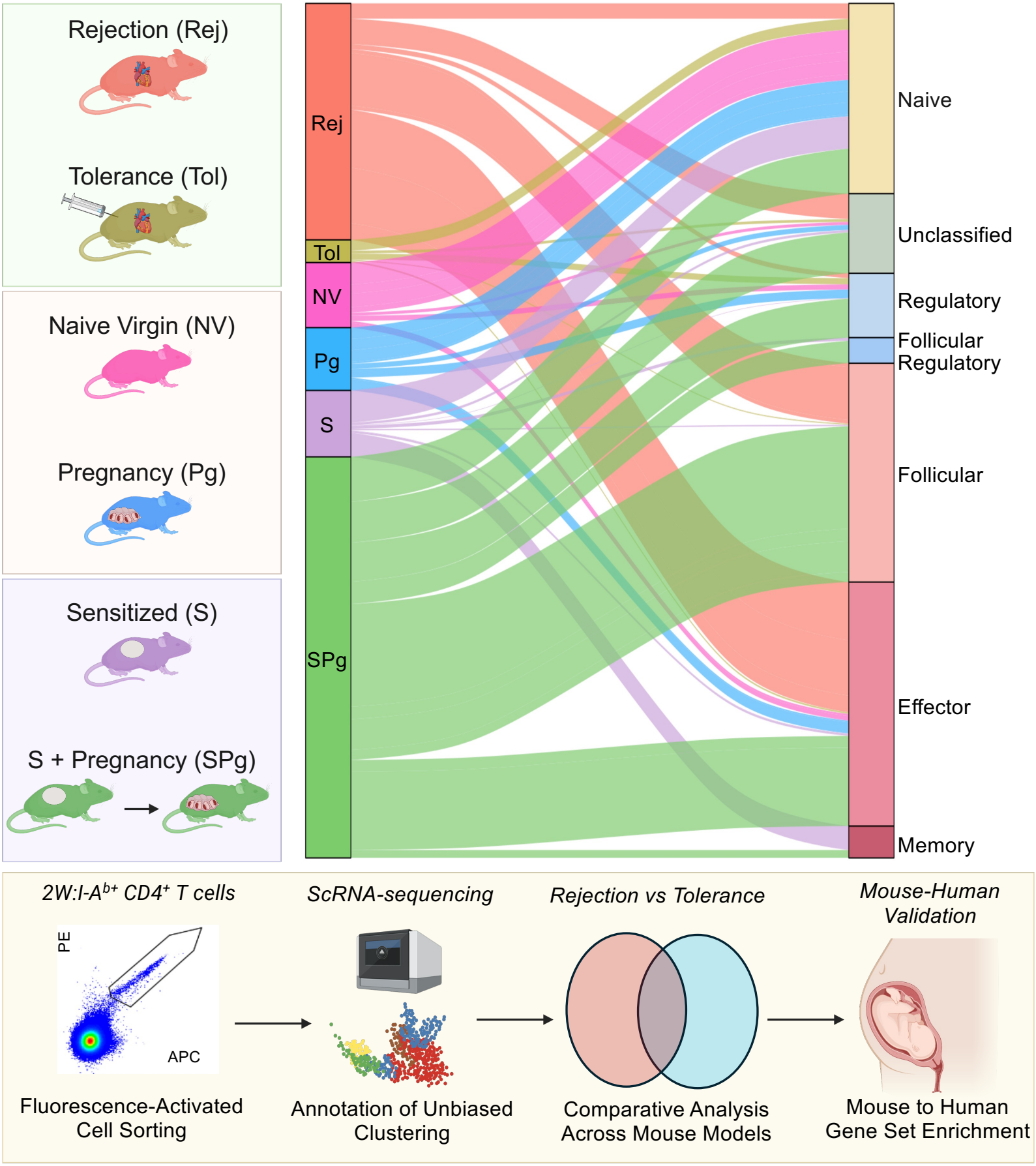
Rejection (Rej)
Tolerance (Tol)
Naive Virgin (NV)
Pregnancy (Pg)
Sensitized (S)
S + Pregnancy (SPg)
Rej
Tol
NV
Pg
S
SPg
Naive
Unclassified
Regulatory
Follicular Regulatory
Follicular
Effector
Memory
2W:I-A^{b+} CD4^{+} T cells
PE
APC
Fluorescence-Activated Cell Sorting
ScRNA-sequencing
Annotation of Unbiased Clustering
Rejection vs Tolerance
Comparative Analysis Across Mouse Models
Mouse-Human Validation
Mouse to Human Gene Set Enrichment

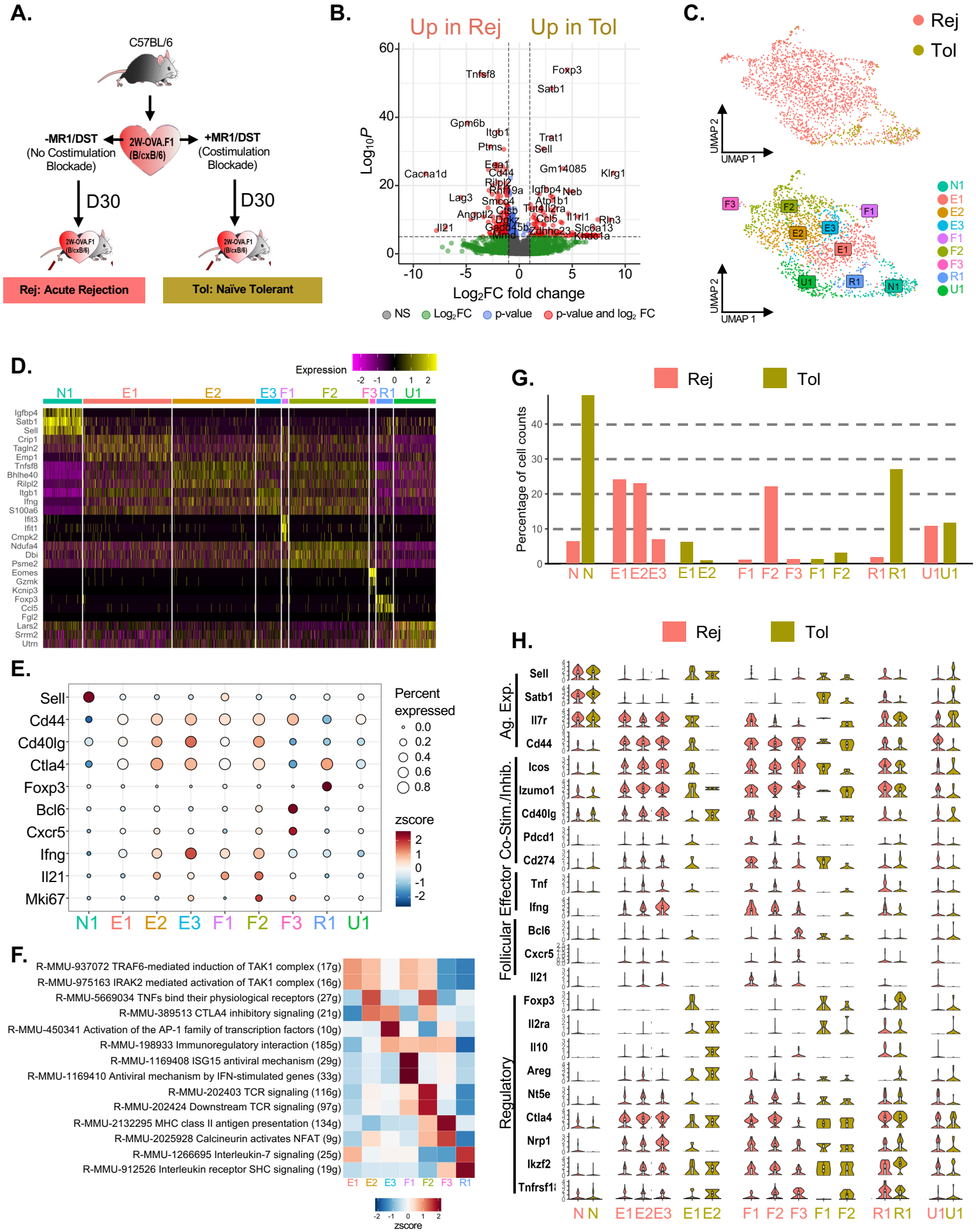

Andrade, et. al, Fig.1

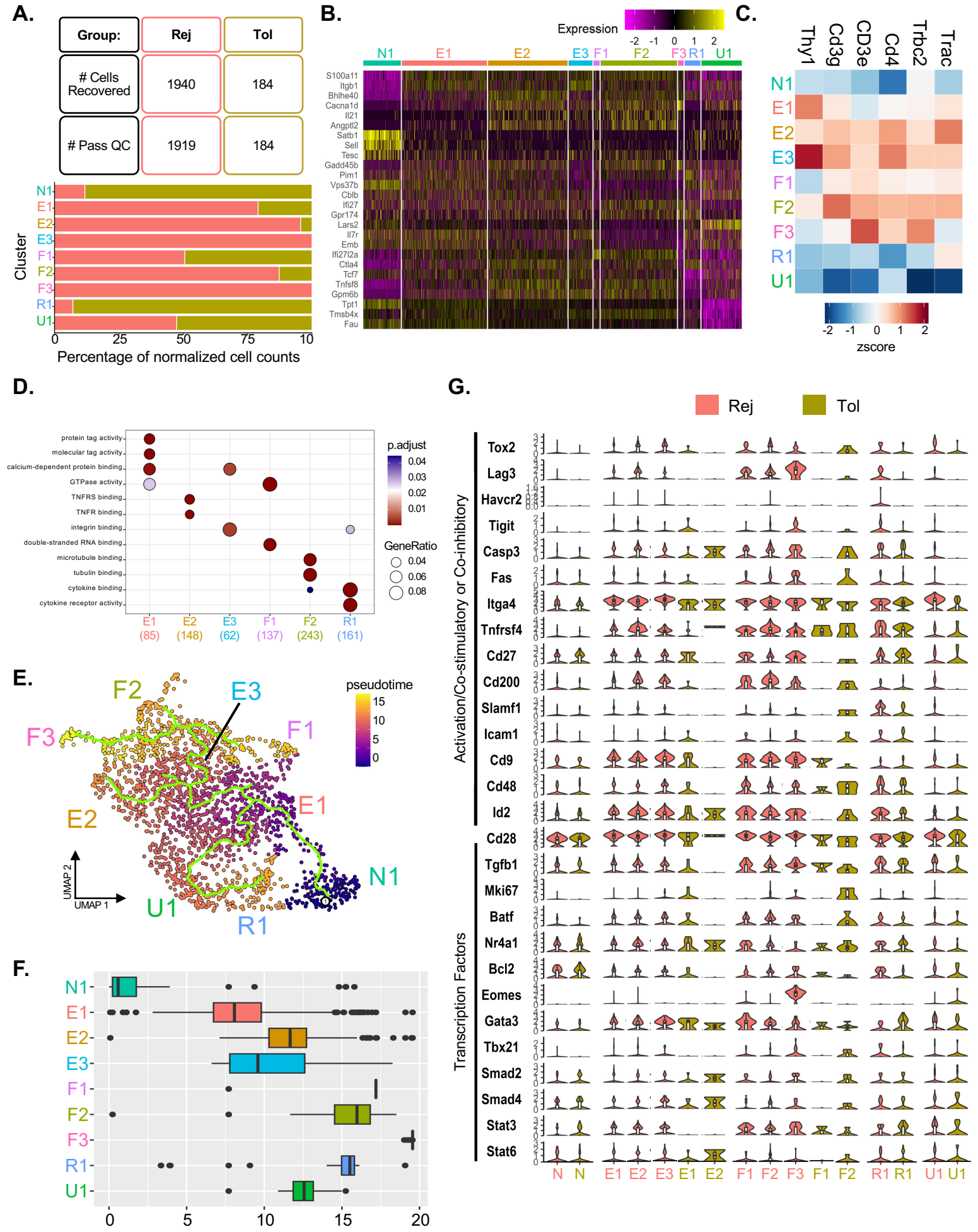

Andrade, et. al, Supplemental Fig. 1

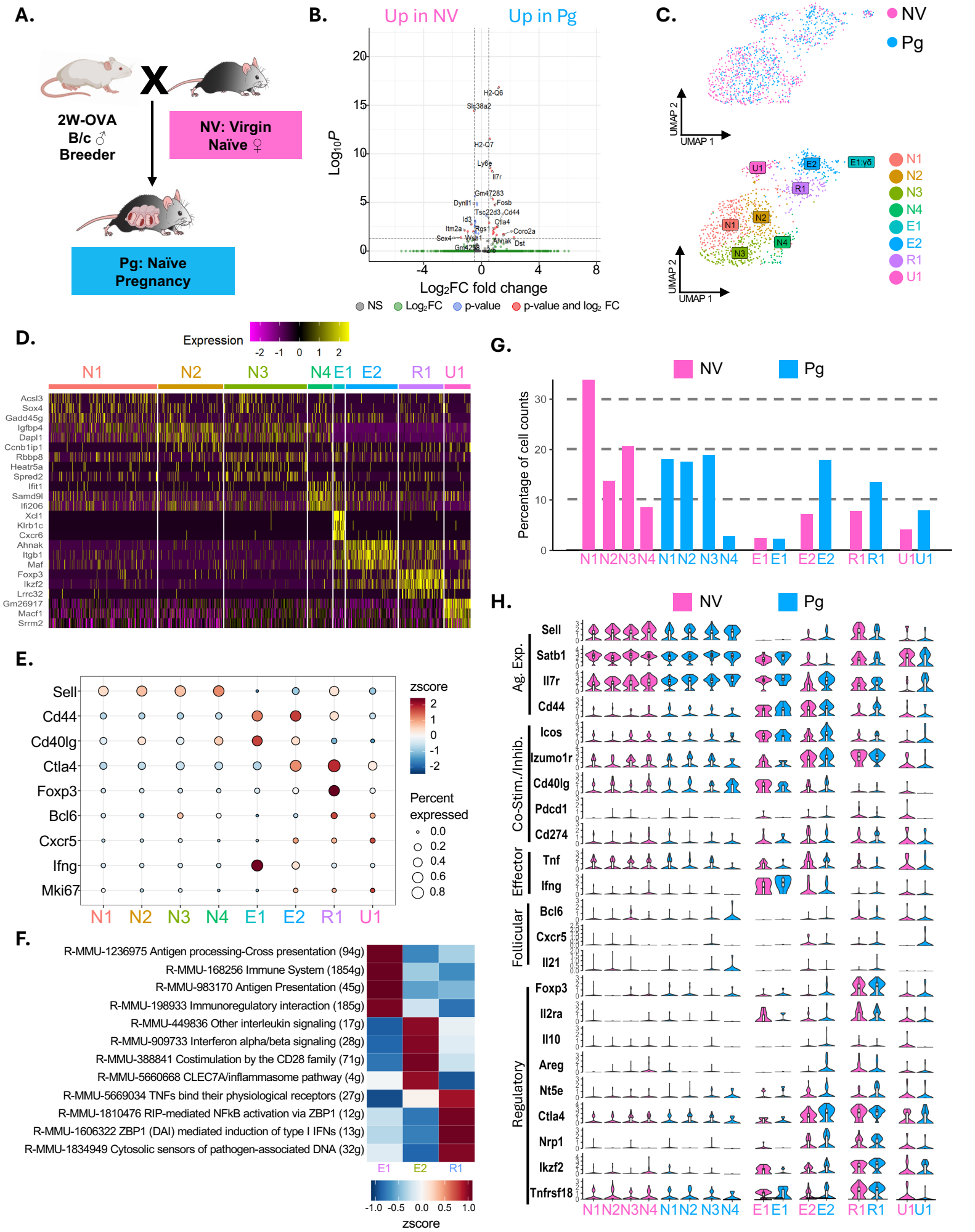

Andrade, et. al, Fig.2

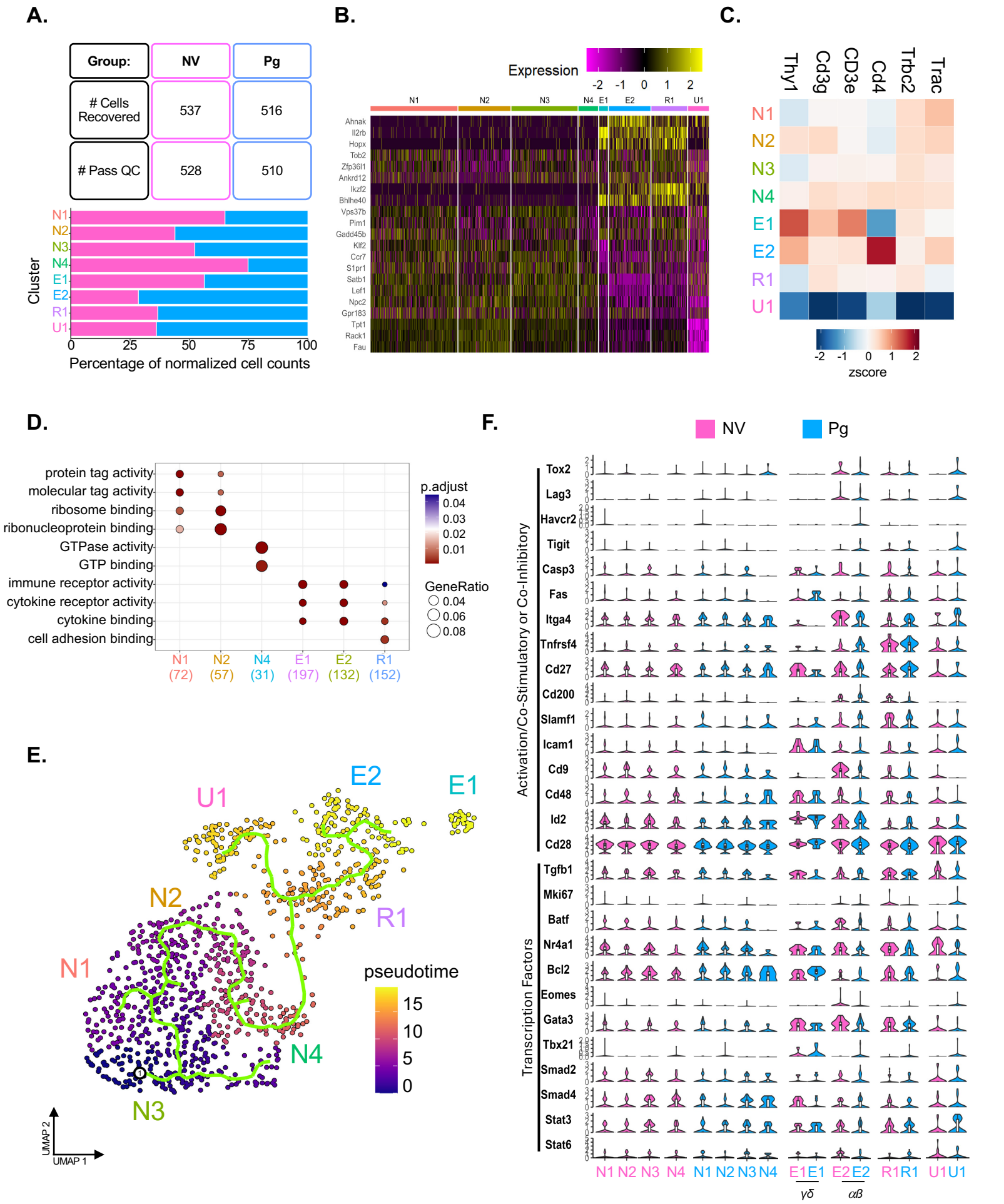

Andrade, et. al, Supplemental Fig. 2

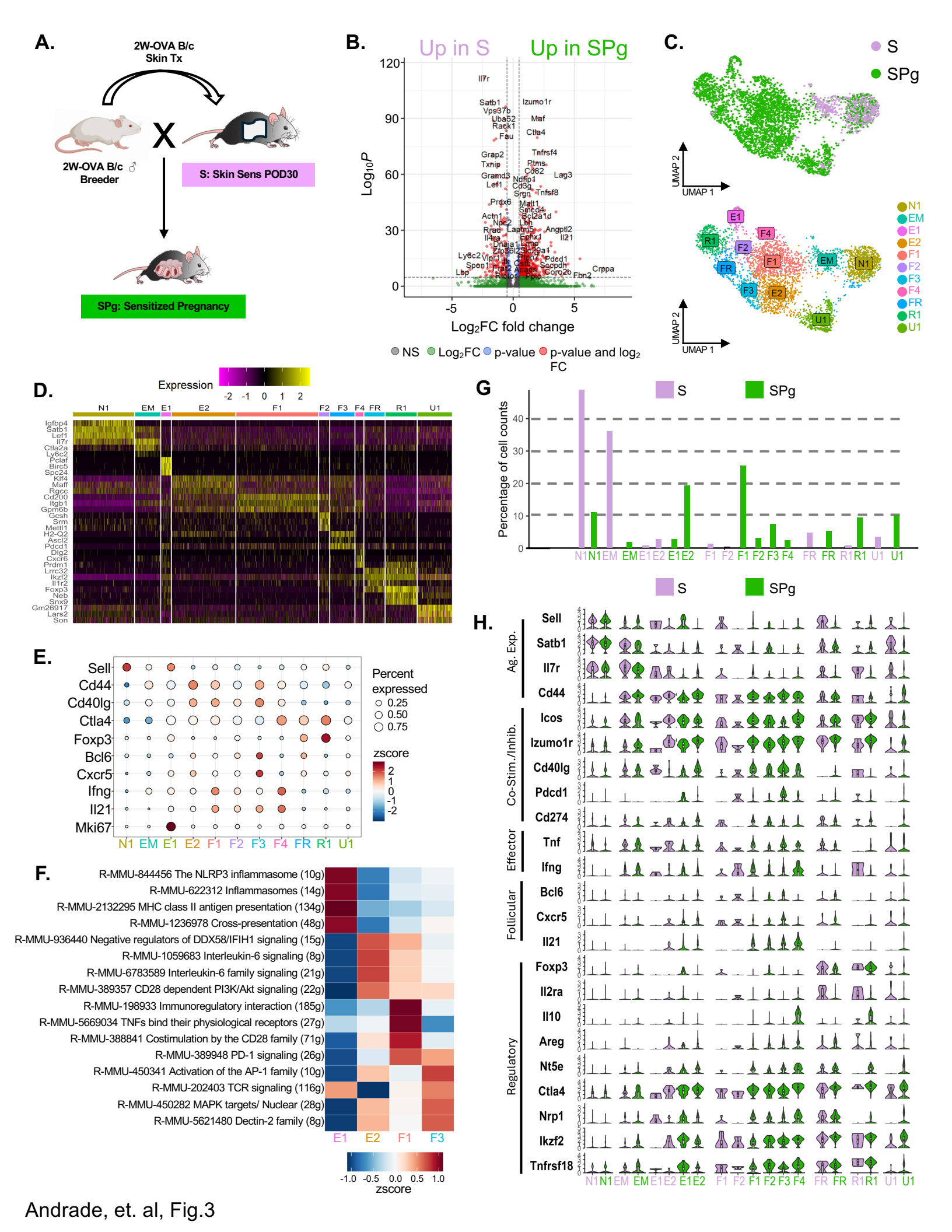

Andrade, et. al, Fig.3

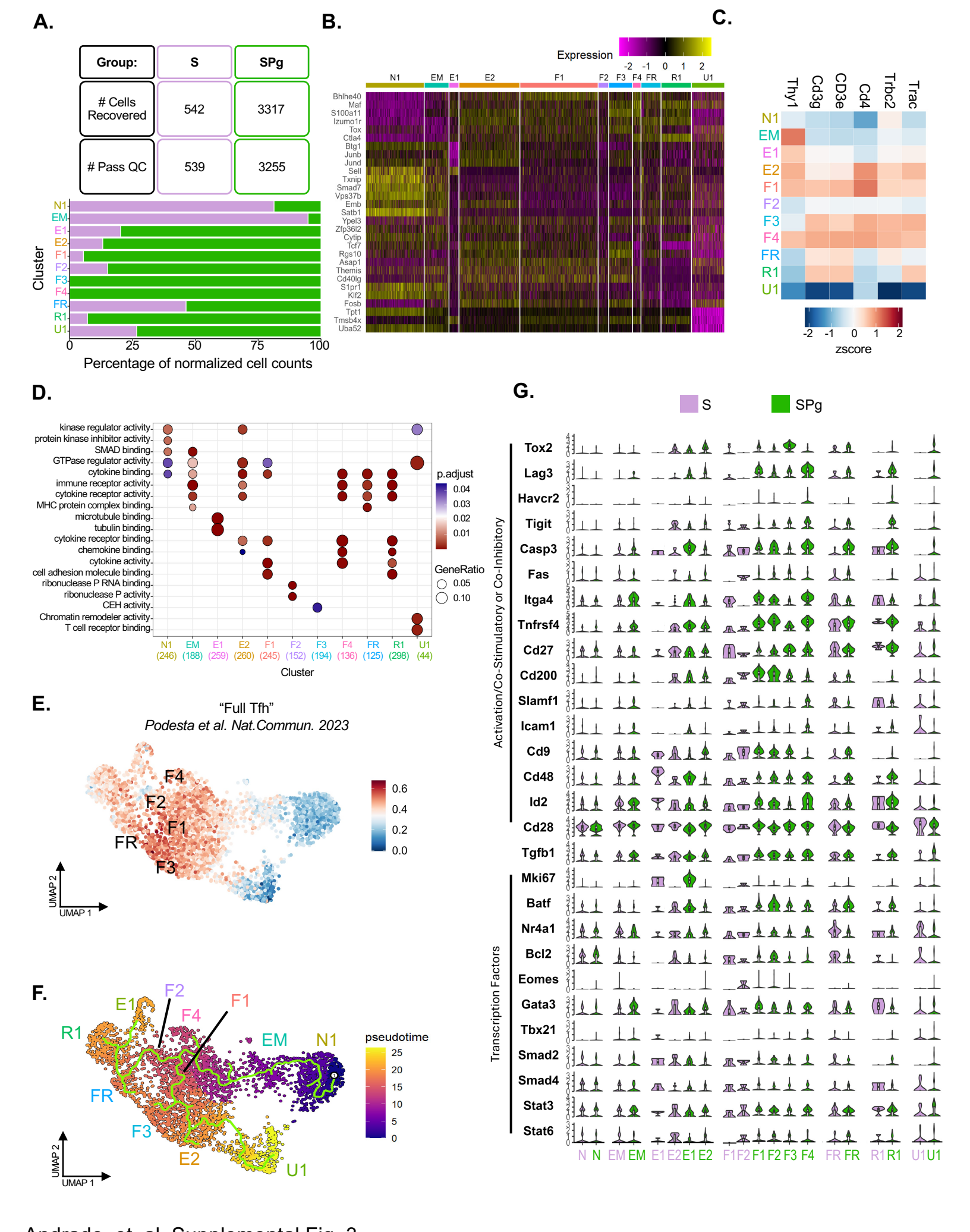

Andrade, et. al, Supplemental Fig. 3

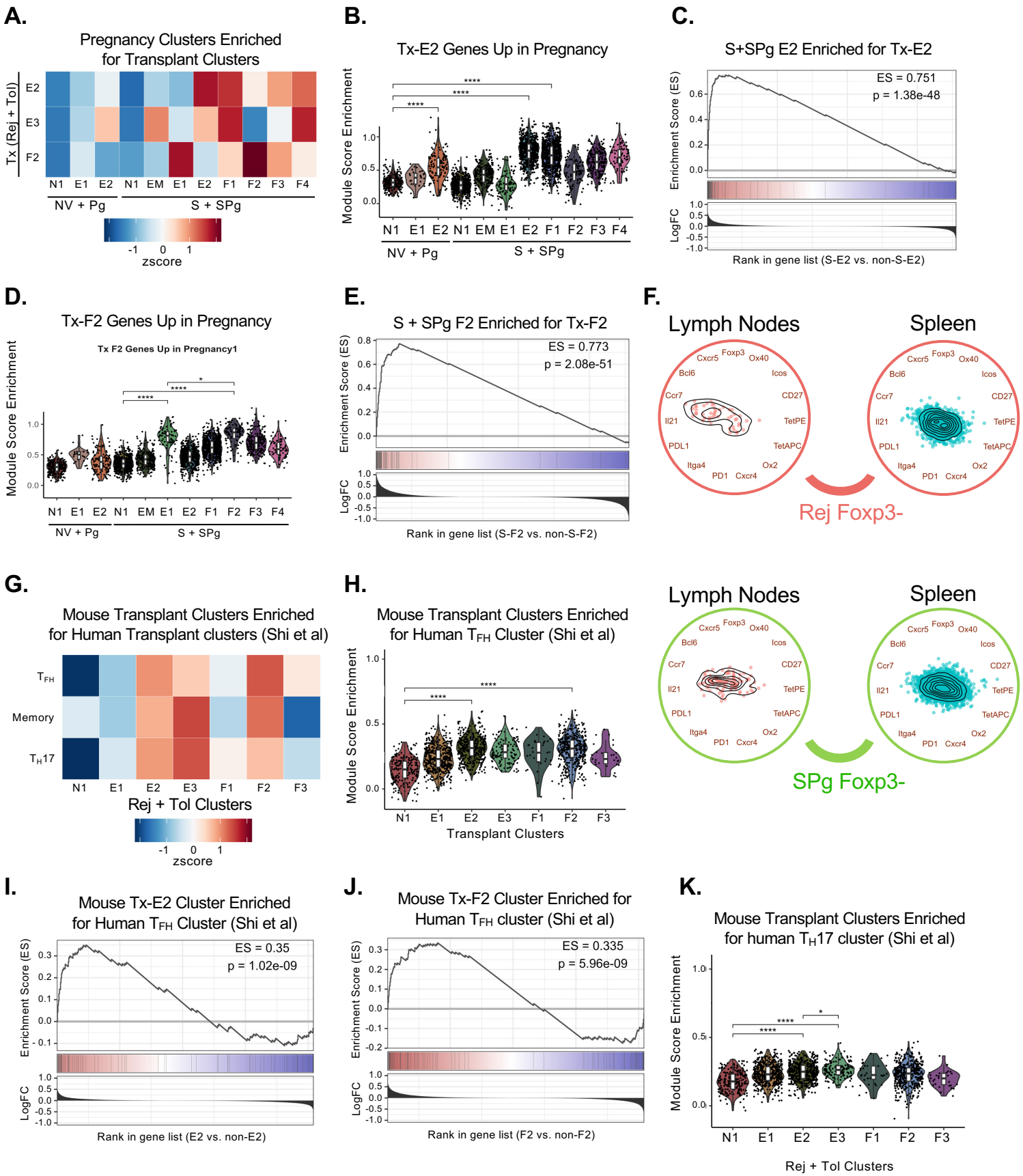

Andrade, et. al, Fig.4

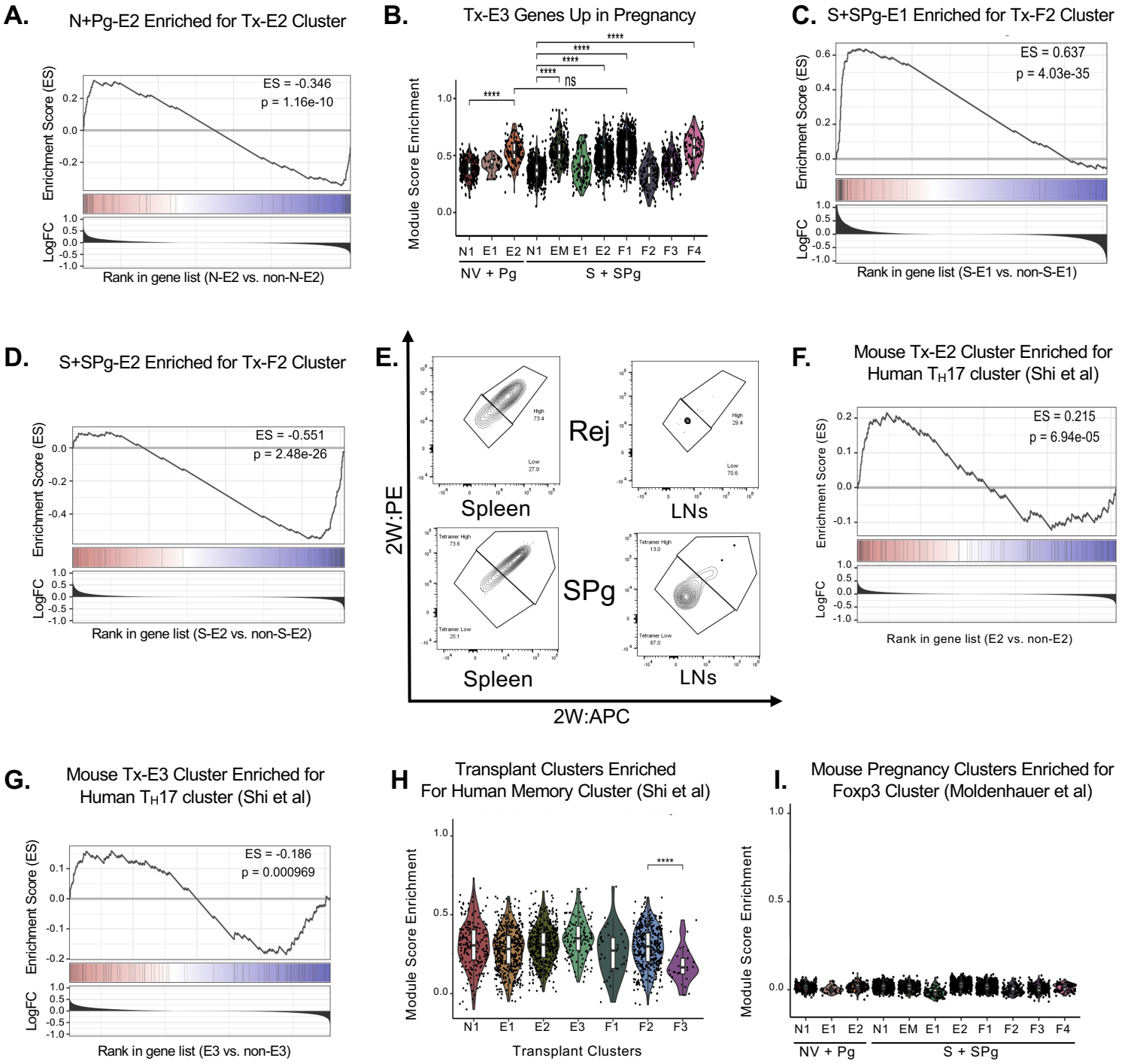

Andrade, et. al, Supplemental Fig.4

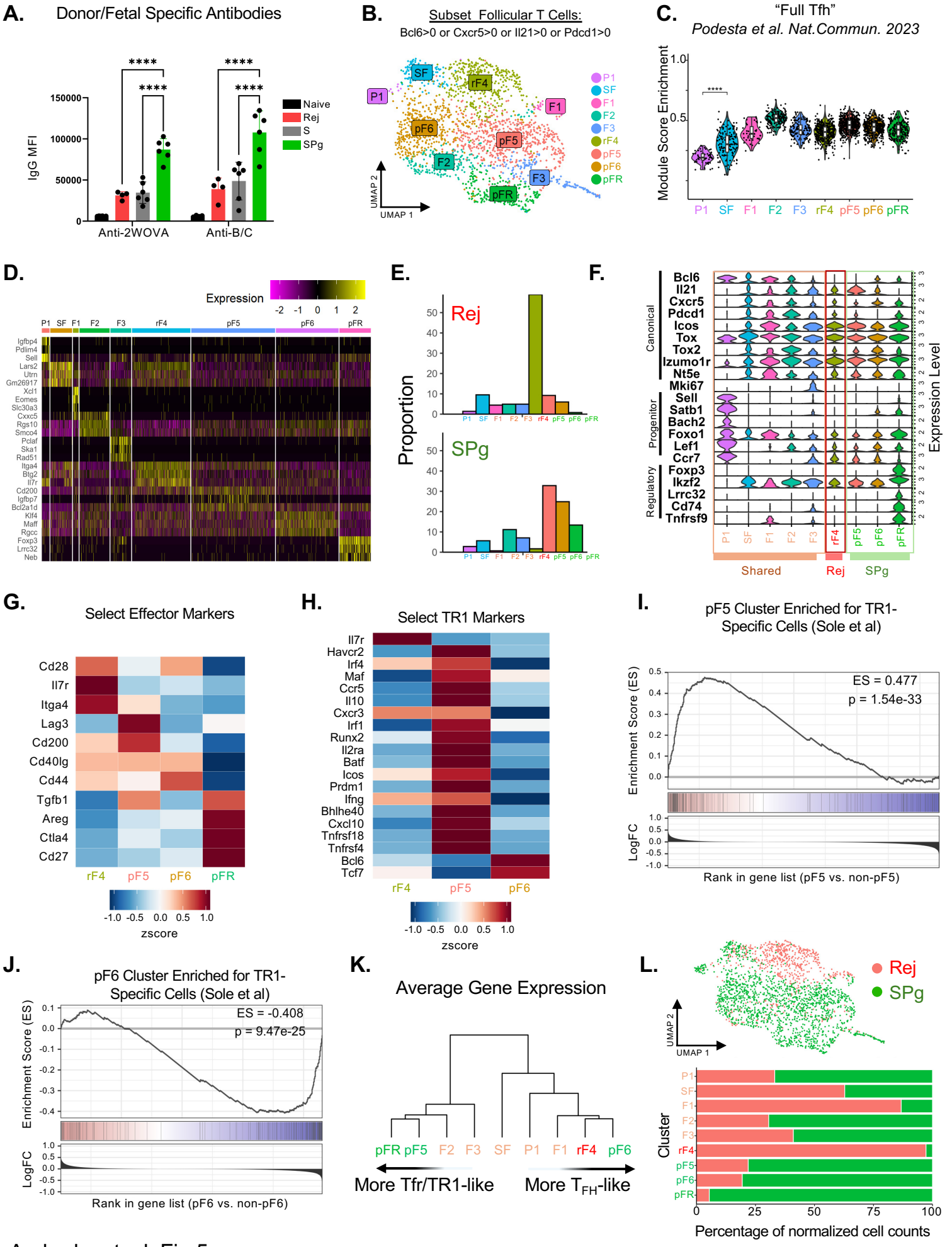

Andrade, et. al, Fig.5

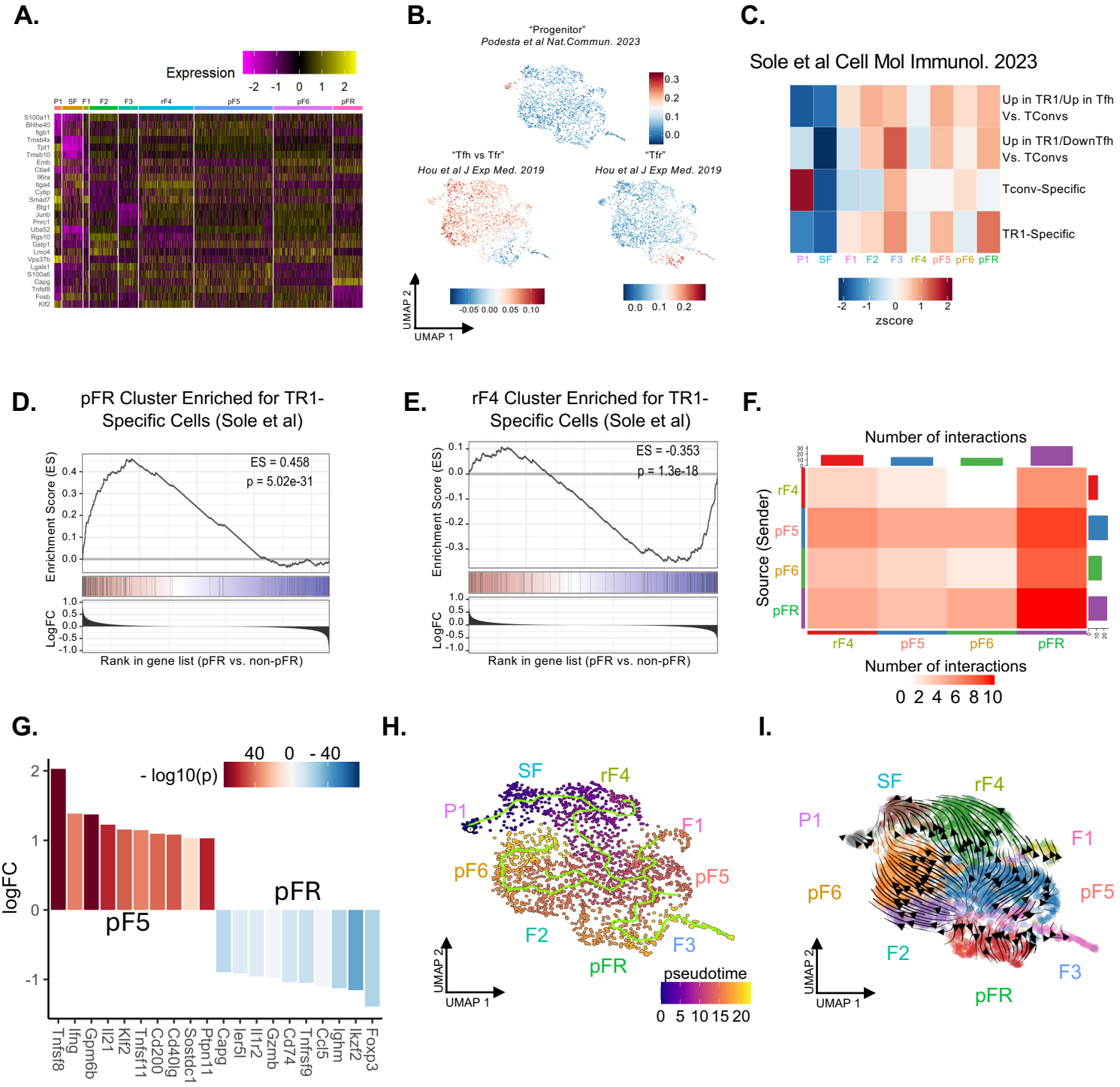

Andrade, et. al, Supplemental Fig. 5

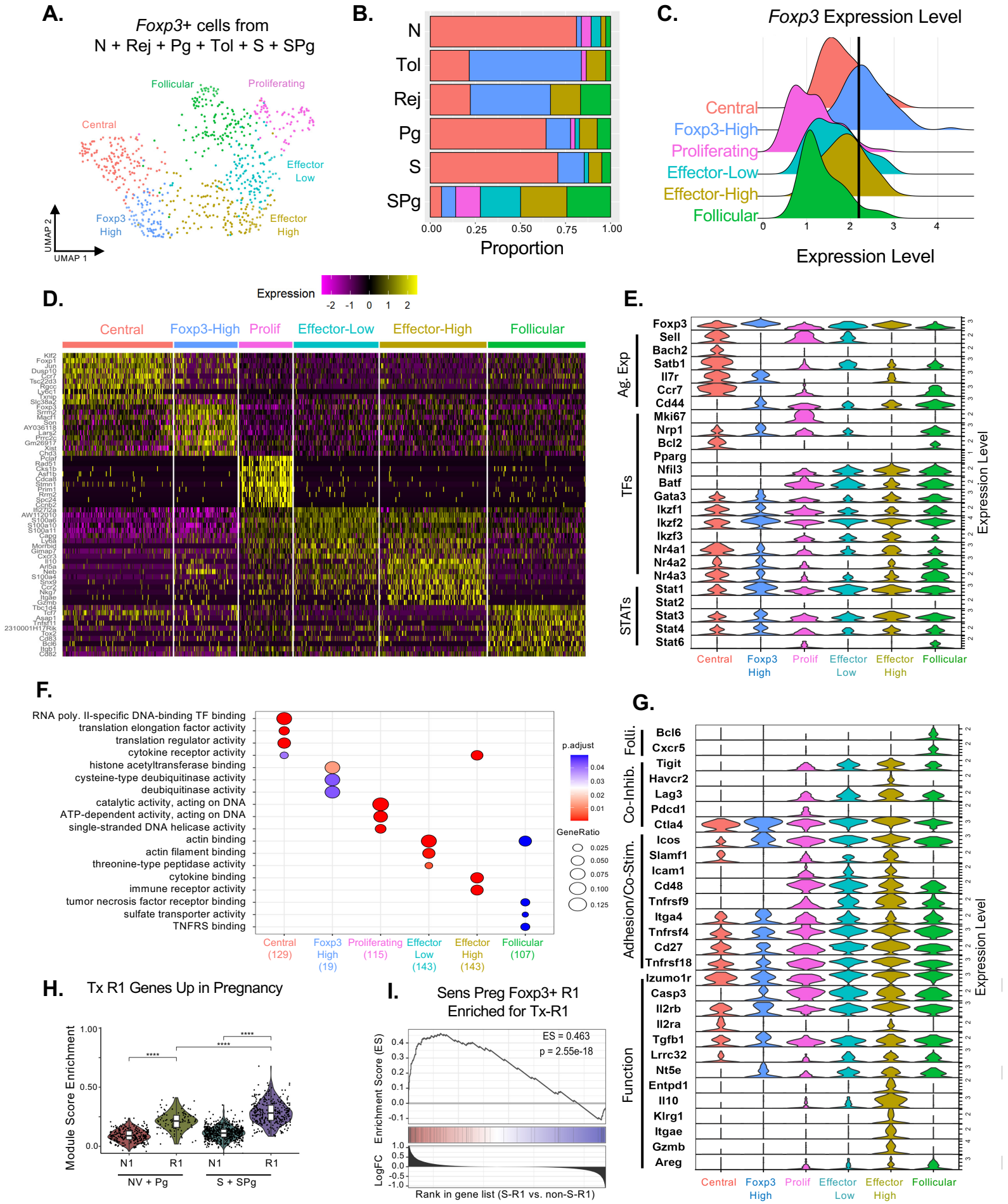

Andrade, et. al, Fig.6

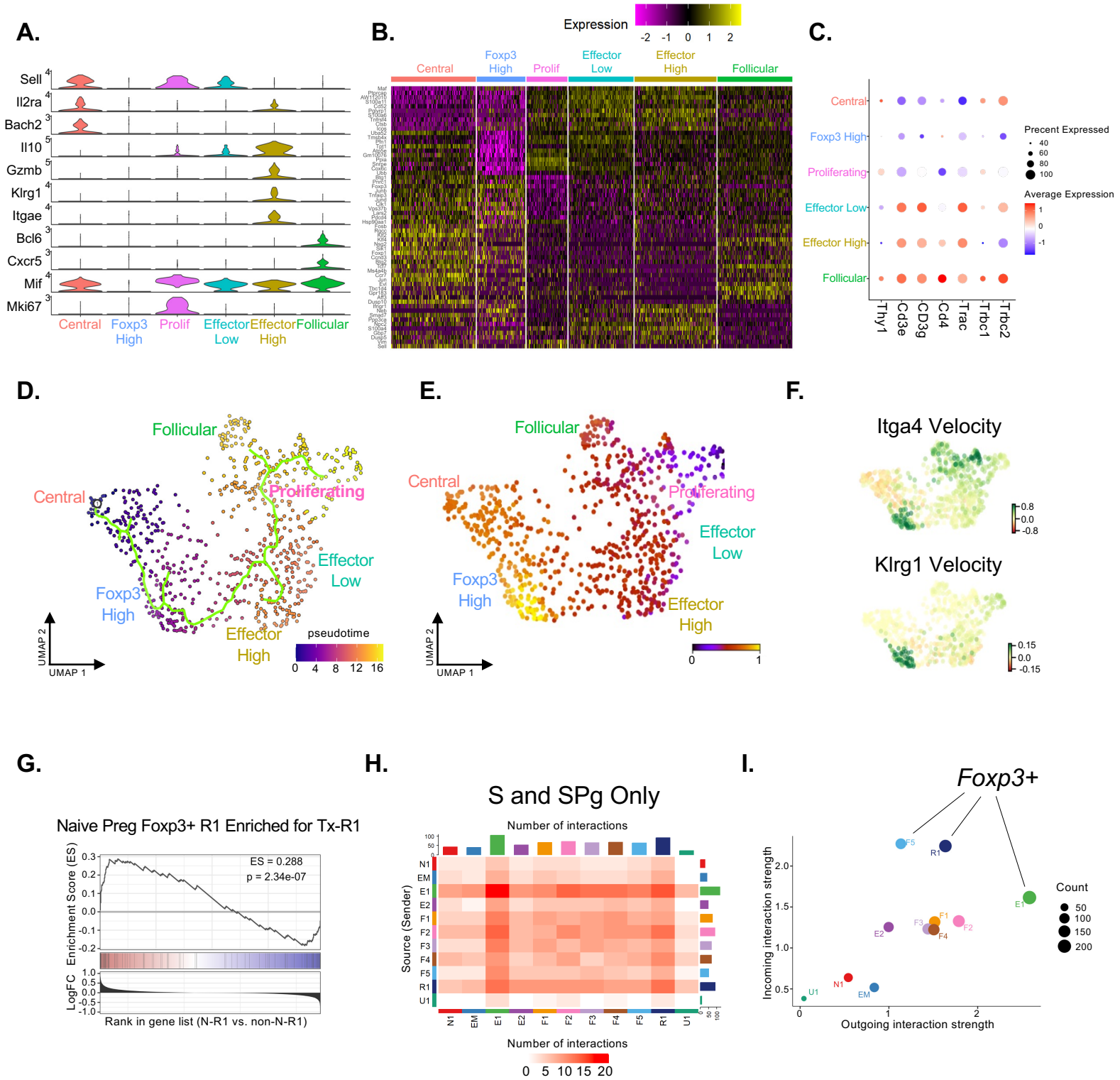

Andrade, et. al, Supplemental Fig. 6

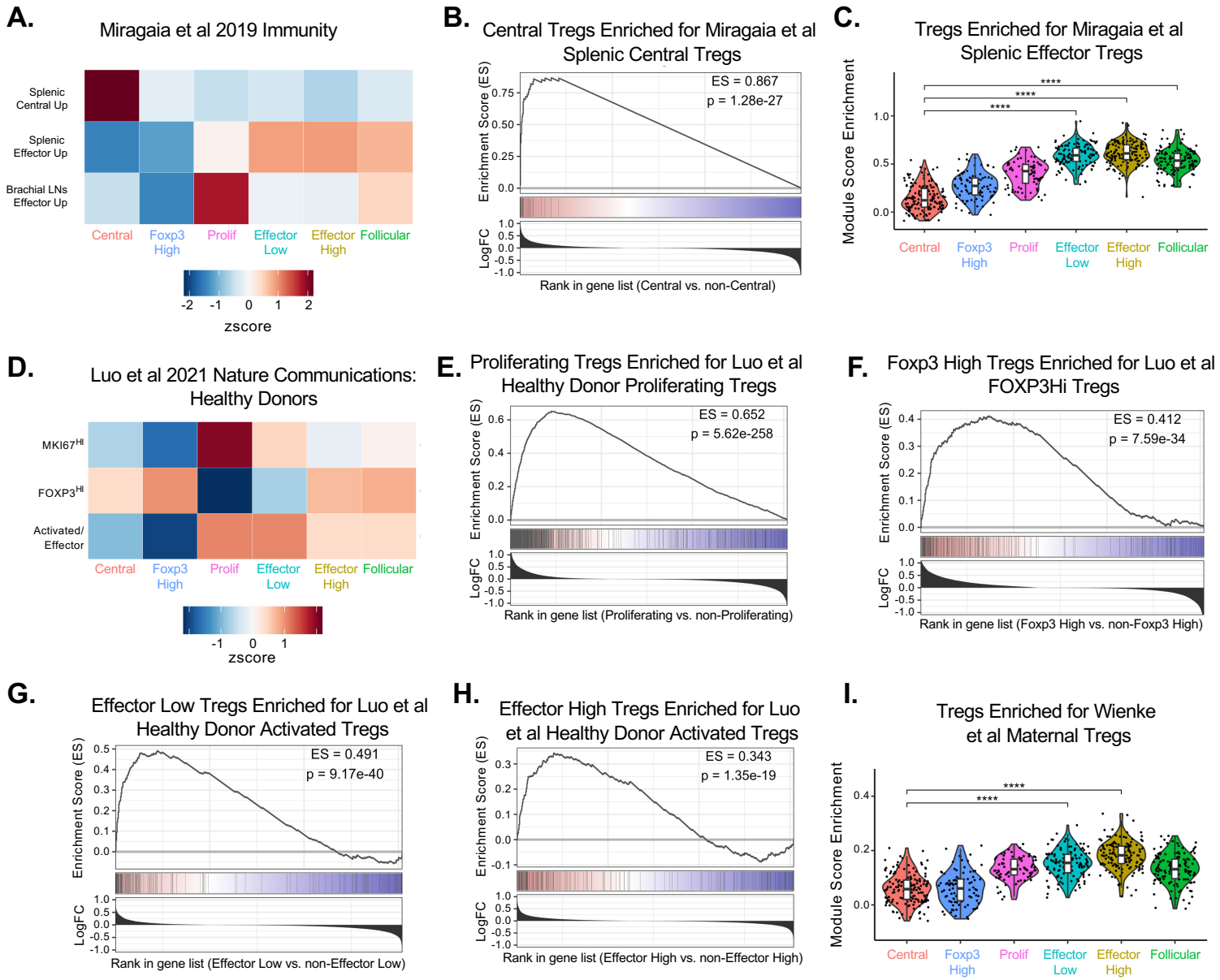

Andrade, et. al, Fig.7

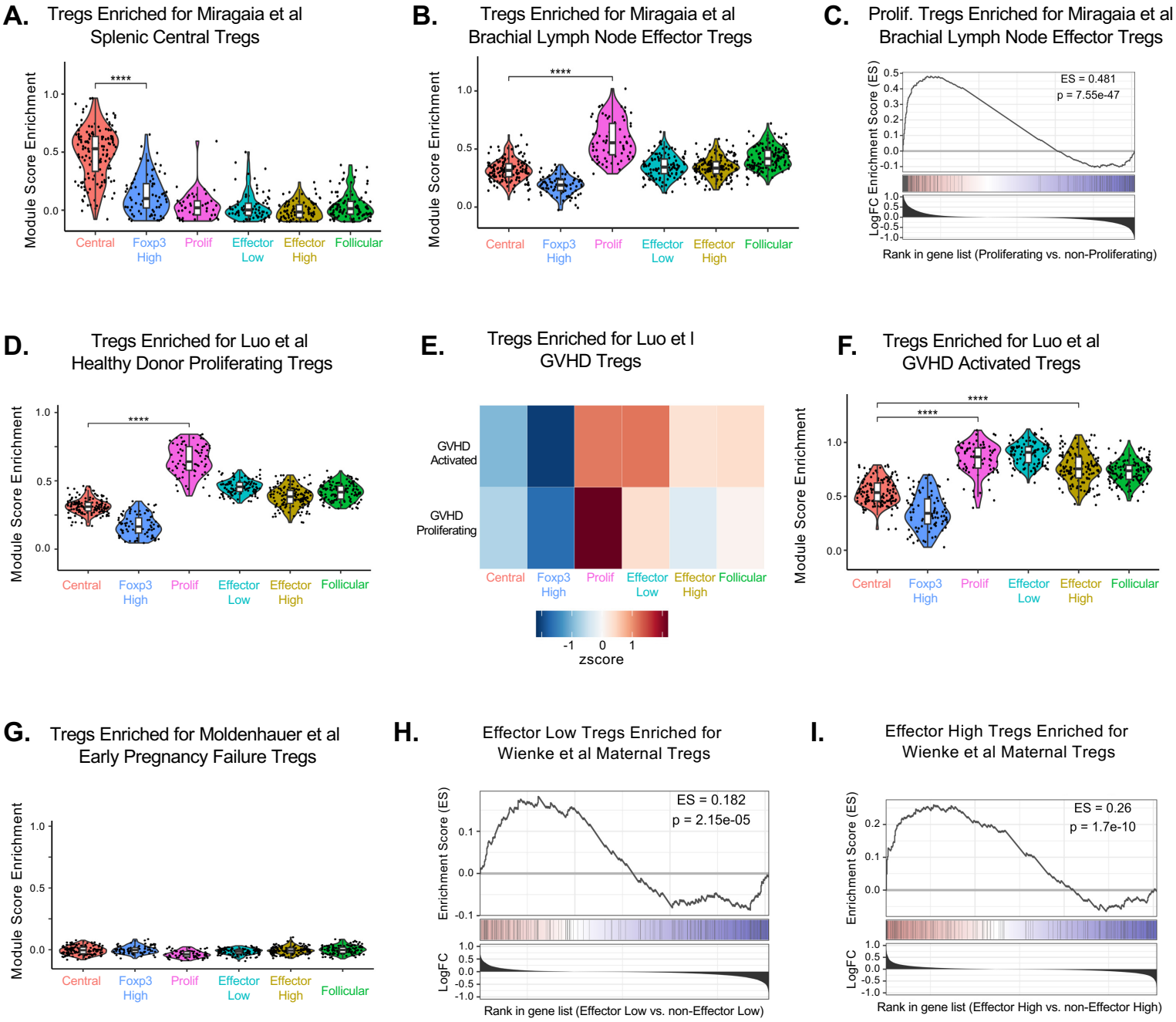

Andrade, et. al, Supplemental Fig. 7